



Automatic generation of knee kinematic models from medical imaging



Beichen Shi (石北辰)^{a,b,*}, Martina Barzan^{a,b}, Azadeh Nasseri^{a,b}, Jayishni N. Maharaj^{a,b}, Laura E. Diamond^{a,b}, David J. Saxby^{a,b}

^a Griffith Centre of Biomedical and Rehabilitation Engineering, Menzies Health Institute Queensland, Gold Coast campus Griffith University QLD 4222, Australia

^b School of Health Sciences and Social Work, Gold Coast campus Griffith University, Parklands Dr Southport QLD 4222, Australia

ARTICLE INFO

Keywords:

Paediatric
Computational
Magnetic resonance imaging
Parallel mechanism
Validation
Biomechanics

ABSTRACT

Background and Objective: Three-dimensional spatial mechanisms have been used to accurately predict passive knee kinematics, and have shown potential to be used in optimized multibody kinematic models. Such multibody models are anatomically consistent and can accurately predict passive knee kinematics, but require extensive medical image processing and thus are not widely adopted. This study aimed to automate the generation of kinematic models of tibiofemoral (TFJ) and patellofemoral (PFJ) joints from segmented magnetic resonance imaging (MRI) and compare them against a corresponding manual pipeline.

Methods: From segmented MRI of eight healthy participants (four females; aged 14.0 ± 2.6 years), geometric parameters (i.e., articular surfaces, ligament attachments) were determined both automatically and manually, and then assembled into TFJ and PFJ kinematic models to predict passive kinematics. The TFJ model was a six-link mechanism with deformable ligamentous constraints, whereas PFJ was a modified hinge. The ligament length changes through TFJ flexion were prescribed to literature strain profile. The geometric parameters were optimized to ensure physiological kinematic predictions through a Multiple Objective Particle Swarm Optimization.

Results: Geometric parameters showed strong agreement between automatic and manual pipelines (median error of 2.8 mm for anatomical landmarks and 1.5 mm for ligament lengths). Predicted TFJ and PFJ kinematics from the two pipelines were not statistically different, except for tibial superior/inferior translation near terminal TFJ extension. The TFJ kinematics predicted from the automatic pipeline had mean errors of 3.6° and 12.4° for adduction/abduction and internal/external rotation, respectively, and <7 mm mean translational error compared to the manual pipeline. Predicted PFJ had $<9^\circ$ mean rotational errors and <6 mm mean translational errors.

Conclusions: The automatic pipeline developed and presented here can predict passive knee kinematics comparable to a manual pipeline, but removes laborious manual processing and provides a systematic approach to model creation.

1. Introduction

Kinematic models of the knee predict the relative motions between femur and tibia (and patella for specific models). These models vary in complexity and anatomical fidelity, ranging from simple spherical or hinge [27] joints, to two-dimensional planar mechanisms [45], and three-dimensional (3D) spatial parallel mechanisms [17,35,36,40]. Spatial parallel mechanisms can accurately predict passive kinematics of the tibiofemoral (TFJ) and patellofemoral (PFJ) joints [40]. They can also be highly personalised using medical imaging [3,9,34]. Spatial parallel mechanisms are efficient alternatives for predicting knee joint

kinematics compared to more complex and computationally expensive models used through finite element analysis [16,44].

Spatial parallel mechanisms require tuning of their geometric parameters to ensure a match between their predicted kinematics and the subject's experimentally measured motions [34,39,40] or to respect literature values [3,9]. Recently, methods that predict natural knee motion (under physiological loading) based on a static joint geometry have shown promise [14,15]. Conconi et al. [14] proposed a method to compute TFJ kinematics by maximizing joint congruence (i.e., minimizing peak contact pressure) which was based on articular surfaces with idealized articulation. Another recent study reconstructed *in vitro*

* Corresponding author at: School of Health Sciences and Social Work, Griffith University, Gold Coast campus, Parklands Dr Southport QLD 4222, Australia.

E-mail address: beichen.shi@griffithuni.edu.au (B. Shi).

TFJ motion in one specimen by optimizing alignment between the instantaneous helical axis of rotation and joint constraints [15]. This showed potential to predict accurate knee kinematics through generic assumptions about articular constraints and warrants further investigation.

Knee kinematic models based on spatial parallel mechanisms have been tested in multibody kinematic optimization and are preferable to simplistic (e.g., spherical) joint models [12,21]. These kinematic models with anatomical basis enable computation of ligamentous constraint forces as well as medial and lateral contacts in subsequent multibody optimization [32], and can be extended to kinetostatic modelling to study ligament and contact forces under loaded conditions [42]. However, these kinematic models have been impractical to implement outside research settings (e.g., in clinics) or at scale (e.g., large cohorts) due to resource demands (i.e., acquisition of medical imaging, image processing, model development, model use). To render spatial parallel mechanisms of the knee viable for routine clinical use or for large trials, automatic model development is crucial.

Development of a personalised spatial parallel mechanism requires an individual's joint anatomy derived from medical imaging (e.g., magnetic resonance imaging (MRI)). Automatic segmentation of knee bones and cartilages from MRI is an emerging technology [20,26,37]. After segmentation, geometric parameters defining the mechanism (e.g., anatomical landmarks, articular surfaces) are manually determined. This can take upwards of 30 min and relies on the expertise of a trained operator. Automatic determination of geometric parameters using geometric analyses [24,31,38,43], atlas-based methods [8,23], and neural networks [29] have been applied to several bones of the lower body (e.g., pelvis, femur, tibia). Geometric analyses extract shape features by analysing local curvature [43], principal axis of inertia, shape principal components, cross-sectional area, or 3D convex hull [24,31,38], and are interpretable as they follow intuitive procedures to extract features of interest. Atlas-based methods morph a template atlas previously defined onto novel anatomy [8,23], which aids determination of landmarks with ambiguous shape features that might elude geometric analysis. Although neural network methods have shown high accuracy in landmark detection in different bones and capability to handle geometrically complex landmarks, they generally require large (manually annotated) training data [11,30]. Overall, automated approaches can achieve better or comparable results to manual determination of geometric parameters, and critically, are not subject to human operator variability [8,19,23,29,31,38]. However, no study has assembled knee kinematic models based on parallel mechanism from automatically determined geometric parameters.

Recently, Modenese and Renault [31] developed an automatic pipeline to assemble lower limb (articulated) skeletal models using models of a subject's bones. Their approach was shown robust for adult anatomy, but is untested in paediatric populations and implemented a simplified knee kinematic model (e.g., hinge TFJ) without a PFJ. To date, no study has assessed a fully automated pipeline to assemble subject-specific knee (i.e., TFJ and PFJ) kinematic models based on spatial parallel mechanisms developed from MRI segmentation. This study aimed to determine the accuracy of paediatric TFJ and PFJ models assembled using automated determination of geometric parameters. The automatic pipeline was evaluated against the manual pipeline for determination of geometric parameters and predicted TFJ and PFJ kinematics. We hypothesised no statistically significant difference in predicted TFJ and PFJ kinematics between automatic and manual pipelines.

2. Methods

2.1. Participants and data acquisition

Data from eight healthy participants (4 females; mean standard deviation: age 14.0 ± 2.6 years, mass 51.1 ± 10.5 kg, height 1.64 ± 0.11 m)

who participated in a previous study at our institution [3] were used in this study. Participant guardians provided written informed consent consistent with the approved study protocol from the Children's Health Queensland Hospital and Health Services human research ethics committee (HREC/13/QRCH/197).

All participants underwent MRI at Queensland Children's Hospital (Brisbane, Australia). A full lower-body scan of participants in supine position was performed using a 1.5 T scanner (Siemens Magneto Avanto, Germany). The MRI was acquired from pelvis to feet with the knee in neutral position (i.e., approximately 0° TFJ flexion) using 3D proton density SPACE sequence with 1.0 mm slice thickness and $0.83 \times 0.83 \times 1.0\text{mm}^3$ voxel size. Bones, cartilage, and ligaments of the knee as well as patellar tendon were segmented manually in Mimics Research v20.0 (Materialise, Belgium) to create 3D surface meshes of each structure.

2.2. Manual and automatic determination of geometries

The TFJ was modelled as a parallel mechanism based on the geometry of the articular surfaces and attachment of ligaments, while the PFJ was modelled as a modified hinge rotating about an axis defined by the femoral condyles (Fig. 1) [3]. The required geometries for the TFJ and PFJ models (Table 1) were determined manually and automatically from the 3D meshes of the knee in the neutral position during MRI scan. Anatomical landmarks, ligament attachment regions, and articular surfaces (Table 1) were determined manually using 3-Matic v17 (Materialise, Belgium) by one operator. These same geometries were also determined automatically using established algorithms adapted for our application.

Anatomical landmarks and articular surfaces (Table 1) were automatically determined using the STAPLE toolbox [31,38]. These previously published algorithms for geometric analysis of bone models can be summarized in the following steps: a) initial orientation estimate (e.g., defining longitudinal axis of long bones) via principal inertia axis; b) cross-sectional area analysis to define regions of bone (e.g., distal femur); c) primitive shape fitting to extract local bone features (e.g., sphere of femoral head). Minor tuning (arrived at via trial and error) of two parameters controlling the cutoff of the articular surfaces was performed to ensure good alignment between automatic and manual methods. We added new methods to automatically determine ligament attachments and patellar landmarks. Ligament attachments were determined by fitting centrelines through the vertices of the ligament mesh and extrapolating until intersection with the respective bone mesh. To determine patellar landmarks, we combined an atlas with non-rigid morphing [46] because the available geometric method [38] did not reliably process paediatric patella geometries based on our pilot testing. To do this, we created a mean patella model from the patella models of the eight participants. On the mean model, four patellar landmarks were manually digitised. This atlas (i.e., mean patella with digitised landmarks) was then morphed to best match the target (i.e., participant) bone [46], which also morphed the pre-defined landmarks.

2.3. Subject-specific TFJ and PFJ kinematic models

We implemented the TFJ and PFJ kinematic models that had been previously validated against *in vivo* kinematics measures [3]. The TFJ was modelled as a six-link parallel mechanism (Fig. 2). It consisted of two pairs of sphere-on-sphere rigid contacts between femoral and tibial condyles (approximated by best-fit spheres) and four deformable ligamentous constraints representing ACL, PCL, MCL, and LCL, as per [3]. Femur and tibia were assumed to make rigid contact throughout TFJ flexion, which was enforced by a distance constraint between the two pairs of sphere centres. The femoral, tibial, and patellar articular surfaces were approximated by best-fit spheres. Initial ligament and patellar tendon lengths were calculated from their attachments on the respective bone surfaces (i.e., distance from origin to insertion) in neutral knee position. Ligament length changes throughout TFJ flexion

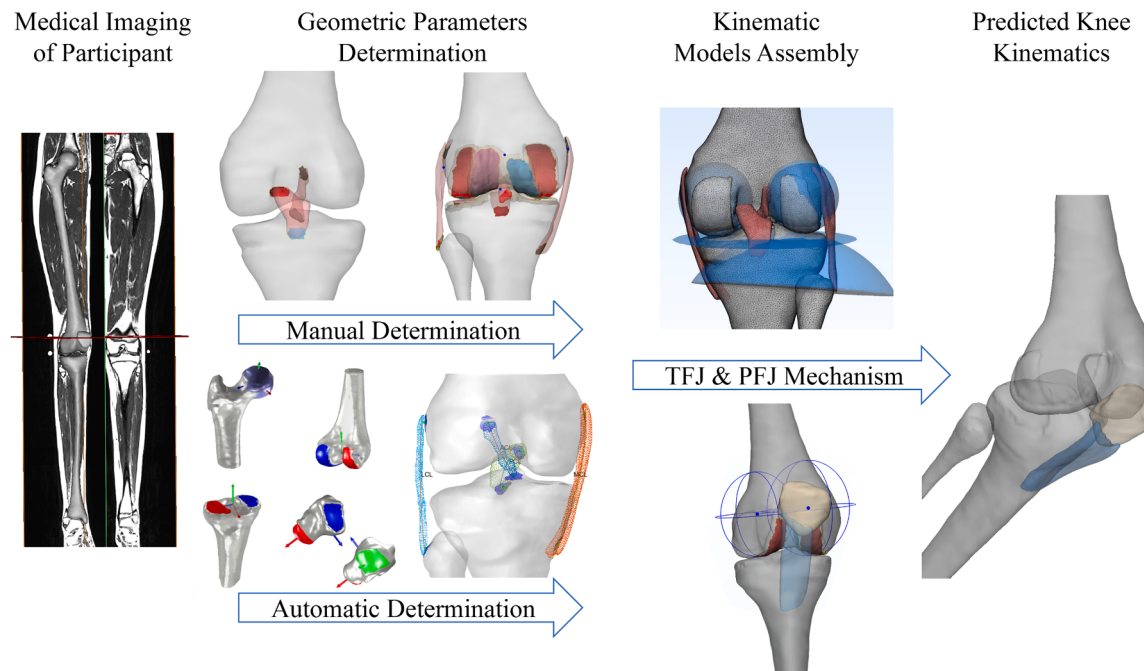


Fig. 1. Workflow diagram showing the automatic and manual pipeline for creating the tibiofemoral and patellofemoral joint kinematic models. Automatic determination of articular surfaces and anatomical landmarks used the STAPLE toolbox [31,38].

Table 1

Geometric parameters used in tibiofemoral (TFJ) and patellofemoral (PFJ) joint models.

Joint	Geometric parameters	Definition
TFJ	Femoral articular surfaces	Medial and lateral condyles of femur articulating with tibia during knee flexion
	Tibial articular surfaces	Medial and lateral tibial plateaus articulating with femoral condyles during knee flexion
	Ligamentous attachments	ACL, PCL, MCL, and LCL attachment sites on femur, tibia, and fibula bone surfaces
	Femoral epicondyles	Bony prominence on medial and lateral epicondyles of femur
	ACL attachments	ACL attachment regions on femur and tibia
	PCL attachments	PCL attachment regions on femur and tibia
	MCL attachments	MCL attachment region on the femur and tibia
	LCL attachments	LCL attachment region on femur and fibula
	Tibial and fibular malleoli	Most distal points of medial (tibial) and lateral (fibular) malleoli
	Hip joint centre	Centre of sphere best fit to femoral head
PFJ	Tibial joint centre	Most concave point in intercondylar area
	Patellar articular surfaces	Medial and lateral patellofemoral articular surfaces (on the femur)
	Patellar landmarks	Most superior, inferior, medial, and lateral points on patella; Mid-point on (posterior) patellar vertical ridge
	Femoral notch	Femoral intercondylar notch
	Femoral trochlear groove	Patellofemoral articulation on trochlear groove on femoral condyle
	Patellar tendon attachments	Patellar tendon attachment regions on patella and tibia

ACL - anterior cruciate ligament; PCL - posterior cruciate ligament; MCL - medial collateral ligament; LCL - lateral collateral ligament.

were guided by tracking the strain profile measured *in vitro* [5–7]. The PFJ was modelled as a modified hinge joint. The patella rotated about the axis defined by the centre of two best-fit spheres approximating the femoral intercondylar groove. The patellar motion was derived from tibial motion by maintaining constant patellar tendon length [3].

Femur, tibia, and patella segment coordinate systems were defined according to established conventions using anatomical landmarks on

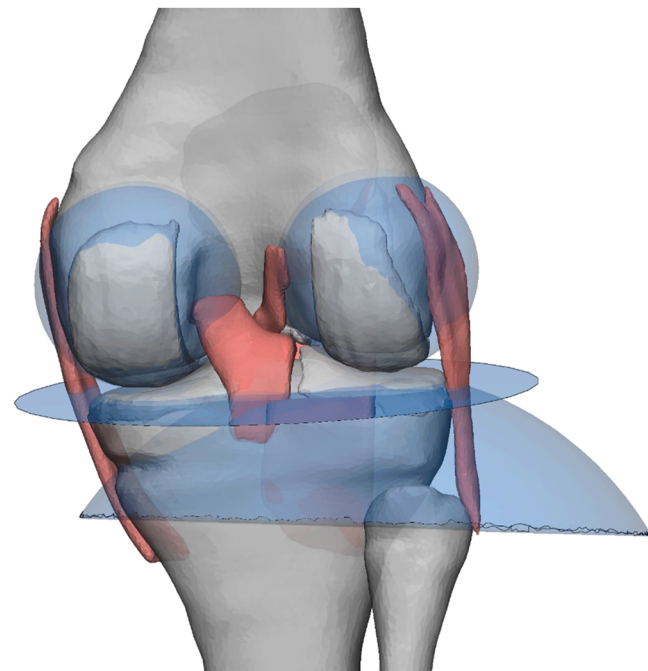


Fig. 2. Visualization of the tibiofemoral joint model (posterior view), consisting of two pairs of sphere-to-sphere contacts and four ligamentous constraints.

bone surfaces [4,10]. Joint kinematics were expressed as ordered rotations: flexion/extension, internal/external, and adduction/abduction [22]. The TFJ mechanism solved six closure equations (i.e., two rigid contact constraints and four ligamentous constraints at prescribed length) given TFJ flexion angle as independent degree of freedom (DOF) from 0° to 90° at 1° increments predicting all dependent DOF [3,9,39]. The closure equations were solved using *fsove* in Matlab (Mathworks, USA) with the Levenberg-Marquardt method. To ensure the mechanism produced a valid solution (i.e., solved without discontinuity) across the

range of motion of interest, the geometric parameters needed to be optimized [3].

A Multiple Objective Particle Swarm Optimization (MOPSO) [13] was implemented to optimize the geometric parameters of the TFJ (i.e., ligament attachments and tibial sphere centres). The MOPSO iteratively updated geometric parameters such that the mechanism derived physiological solutions across the range of motion by concurrently optimizing the following objectives: a) match the pattern between model-predicted and *in vitro* measured kinematics [35,39,40]; b) minimize the difference between optimized and initial MRI-measured geometric parameters (i.e., maintain subject-specificity); c) minimize the range of motion of the predicted TFJ adduction/abduction ($<17^\circ$) and internal/external rotation ($<35^\circ$) if it exceeded the reference values [28]; d) reversal of screw home motion (i.e., tibial internal rotation during initial 30° of TFJ flexion) [25,33]. The MOPSO generated a collection of Pareto solutions (i.e., non-dominant solutions). The selection of the optimal from the Pareto solutions was based on a constraint method, where the best-matched TFJ kinematics (objective a) was selected. The constraints ensured the potential solutions were within or minimally exceeded ($<5^\circ$) the reference range of motion (objective c) and exhibited the reversal of the screw-home motion in the initial 15° of TFJ flexion (objective d).

Similar to TFJ, PFJ geometric parameters were optimized (i.e., sphere centres of femoral condyles and patellar tendon attachment) using MOPSO to achieve two objectives: a) match the pattern between model-predicted and *in vitro* measured kinematics [2,39,40] and b) minimize the difference between optimized and initial MRI-measured geometric parameters. The geometric optimization using MOPSO was largely based on the previous study [3], with the inclusion of the objective d and respective Pareto selection.

2.4. Data analysis and statistics

Automatically determined geometric parameters (Table 1) were compared against their manual counterparts (as ground truth) prior to kinematic model assembly. The corresponding anatomical landmarks and ligament attachments were assessed by Euclidean distance error. The error of corresponding ligament lengths (i.e., the distance between the ligament's two attachments) were also assessed. The articular surfaces were assessed by computing the root mean square error (RMSE) of Euclidean distance of closest point pairs between corresponding surfaces. The residual fitting error measured the fitting quality of the best-fit sphere, calculated as $\frac{1}{n} \sum_{i=1}^n \sqrt{(\| \mathbf{V}_i - \mathbf{c} \| - r)^2}$, where $\mathbf{V}_i (i = 1, \dots, N)$ were the vertices of the articular surface and \mathbf{c} and r were the fitted sphere centre and radius, respectively.

For each participant, the predicted TFJ and PFJ kinematics derived from automatically and manually determined geometric parameters were compared by computing RMSE across the kinematic range of motion (i.e., from 0° to 90° TFJ flexion at 1° increments) for each DOF. Paired *t*-tests, implemented using Statistical Parametric Mapping (SPM1D 0.4, www.spm1d.org), were performed between model-predicted kinematics generated from automatic and manual determination ($p < 0.05$).

3. Results

Automatic determination of the geometric parameters was completed within seconds for each participant, whereas manual determination could take approximately 30 min. Geometric parameter determination errors are reported for ligament attachments, anatomical landmarks, and articular surfaces (Table 2). Ligament attachments were automatically determined with minimal error relative to manual determination (median RMSE: 1.9 mm, interquartile range: 1.8 mm) (Table 2). Consequently, there was a low error in initial ligament lengths compared to lengths derived from manual determination (median

Table 2

Errors between automatic and manual determination of geometry and geometric parameters.

		Median error (IQR) (mm)	Error range [lower, upper] (mm)
Geometric parameter	Ligament attachments	1.9 (1.8)	[0.5, 5.9]
	Anatomical landmarks	2.8 (3.3)	[0.1, 30.4]
	Articular surfaces	1.7 (3.3)	[0.5, 9.5]
	Ligament length*	1.5 (1.8)	[0.0, 7.5]
	Automatic sphere fitting†	0.4 (0.4)	[0.1, 0.9]
	Manual sphere fitting†	0.3 (0.2)	[0.1, 0.9]

IQR: Interquartile range.

* Initial ligament length measured from MRI segmentation at neutral knee position.

† Residual fitting errors of the best-fit sphere were reported independently for automatically and manually determined articular surfaces.

RMSE: 1.5 mm). Anatomical landmarks were automatically determined with median errors ranging from 0.3 mm (hip joint centre) to 5.4 mm (femoral notch) compared to manual determination (Appendix Table A1). Articular surfaces were automatically determined with median RMSE of 0.8 and 1.7 mm for femoral and tibial articulations, respectively, at TFJ and 5.3 mm for femoral articulation at PFJ (Appendix Table A3). Articular surfaces were well approximated (low fitting error) by best-fit spheres and fitting errors were similar between automatically and manually determined surfaces (Table 2).

Significant differences were found between TFJ kinematics in tibial superior/inferior translation predicted from automatically and manually determined geometric parameters. At near full TFJ extension (0–20° flexion), there was a significant difference in tibial superior/inferior translation (Fig. 3) between methods (RMSE: 4.7 mm, standard deviation (SD): 3.3 mm), where the automatic pipeline predicted a more inferior tibia. No significant differences in predicted PFJ kinematics from automatic and manual geometric parameters determination were found (Fig. 3). Predicted TFJ kinematics for both automatic (SD: 17.5°) and manual pipelines (SD: 17.5°) showed large variations across subjects for tibial internal/external rotation (Fig. 3).

Compared against the manual pipeline, predicted TFJ kinematics from the automatic pipeline showed the highest error in tibial internal/external rotation (mean RMSE: 12.4°) and tibial medial/lateral translation (mean RMSE: 6.6 mm) (Table 3). The largest errors for the predicted PFJ kinematics were the internal/external rotation (mean RMSE: 8.3°) and medial/lateral translation (mean RMSE: 5.7 mm) (Table 3).

4. Discussion

This study aimed to automatically assemble subject-specific TFJ and PFJ kinematic models using 3D knee joint geometry in a paediatric cohort and compare the performance with corresponding manually-assembled models. Automatically generated TFJ and PFJ models yielded kinematics comparable to their manual counterparts for most DOF (Fig. 3). Geometric parameters, which constitute the TFJ and PFJ models, were automatically determined using geometric analysis and atlas-based fitting and showed strong agreement with their manual counterparts. The automatic pipeline began with the subject's joint geometry segmented from MRI, but future work to integrate automated image processing [20,37] could yield a fully automated pipeline to predict passive knee motion directly from medical imaging. Due to the lack of research on paediatric populations, this study makes an important contribution and demonstrates the feasibility of this pipeline.

Geometric parameters for TFJ and PFJ models determined via geometric analysis and atlas-based fitting showed strong agreement with

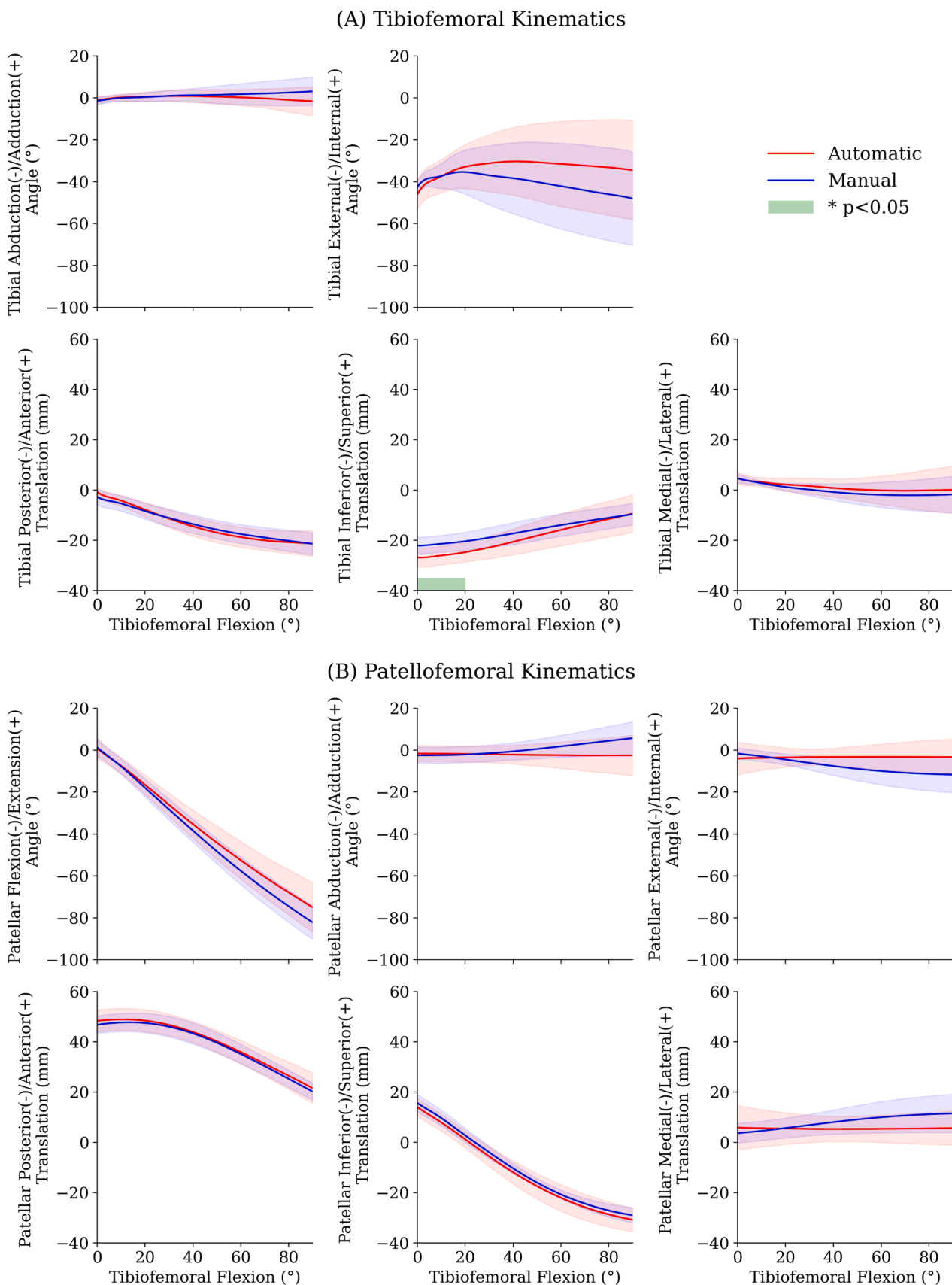


Fig. 3. Model-predicted (A) tibiofemoral (TFJ) and (B) patellofemoral (PFJ) kinematics generated by automatic (red) and manual (blue) determination of knee geometric parameters. Solid lines represent mean values, while shaded areas represent \pm one standard deviation across the tibiofemoral flexion range. The green shaded area on the x-axis indicates a significant difference ($p < 0.05$) assessed using paired t-tests implemented through Statistical Parametric Mapping.

Table 3

Root mean square error (mm) of model-predicted tibiofemoral and patellofemoral kinematics across tibiofemoral flexion range from automatic and manual pipelines for all subjects (mean (standard deviation)). TFJ and PFJ kinematics were expressed as tibial and patellar motions relative to femur, respectively.

	Root mean square error (mm)	
	Tibiofemoral joint	Patellofemoral joint
Extension/flexion (°)	–	6.2 (6.2)
Adduction/abduction angle (°)	3.6 (2.5)	7.9 (5.6)
Internal/external angle (°)	12.4 (9.2)	8.3 (4.0)
Anterior/posterior translation (mm)	4.2 (2.1)	3.5 (2.1)
Superior/inferior translation (mm)	6.4 (2.4)	4.5 (2.9)
Lateral/medial translation (mm)	6.6 (4.5)	5.7 (2.6)

their manually determined counterparts. Ligament attachments were automatically determined with a 1.9 mm median error, resulting in a 1.5 mm median error in overall length. These errors were minimal given average knee ligament length ranges from ~31 mm for PCL and ~73 mm for MCL, meaning length errors were ~5 % in worse cases. Automatic determination of anatomical landmarks generally had higher errors compared to automatic determination of ligament attachments. This discrepancy in error is due to use of centreline fitting for ligaments which makes use of their full geometry and collision detection with their respective bone surface. This approach for ligaments is inherently robust due to averaging effects of centreline tracking and the proximity to bone surface for intersection detection. In contrast, anatomical landmarks were determined using STAPLE [31,38], which defines extrema derived from segment coordinate axes. This approach is sensitive to irregularities on articular surfaces which occur due to errors in image processing. Indeed, femoral notch showed the highest landmark error likely due to its non-unique morphological characteristics, which may cause higher variability in its automatic determination compared to a manual approach.

Overall, automatic determination of patellar articular surfaces showed higher errors compared to femoral and tibial articular surfaces (Appendix Table A3) due to the automatic method consistently selecting larger articular regions compared to the manual counterpart. However, the discrepancy in patellar articular surface did not introduce corresponding higher error in geometric parameters (i.e., best-fit spheres) for the PFJ model. Notably, the medial tibial articular surface is relatively flat (low curvature) compared to the other articular surfaces of the knee (Fig. 2). This resulted in the sphere fit to the medial tibia having a large radius and sensitive to surface error, which can bias the fitting and invert the surface orientation. For example, two study participants had their best-fit medial tibial sphere centre on opposite sides of the articular surfaces. However, overall residual fitting errors were low (Table 2) for both automatically and manually determined articular surfaces including the medial tibial articulation, indicating a good approximation of the surfaces. Although considered reliable (0.9 intra-class correlation coefficient for intra-operator assessments) [18,19], manual digitisation has inter-operator (mean) differences of 2.78 mm (max: 11.51 mm) for femoral landmarks and 1.35 mm (max: 3.7 mm) for tibial landmarks [23]. The automatic approach yielded consistent results for a given bone geometry, thus removing human variability while achieving agreement with the manual counterparts at a level similar to inter-operator variability reported in the literature [23]. Moreover, all geometric parameters were automatically determined within seconds for each participant, while manual digitisation can take up to 30 minutes per participant for a trained operator.

Consistent with our hypothesis, model-predicted TFJ kinematics were not significantly different between the automatic and manual pipeline except for tibial superior/inferior translation across a small range (0–20° TFJ flexion) of terminal knee extension (Fig. 3). No between-model significant differences were found for PFJ kinematics (Fig. 3). It is worth noting that no significant difference was found for

kinematics in some DOF with large RMSE due to the large variation of the kinematics (e.g., tibial internal/external rotation), which is discussed in detail later. The discrepancy between the two pipelines at initial TFJ flexion (i.e., around the neutral pose) was likely due to the different joint coordinate systems established by slightly different sets of anatomical landmarks. Model predicted TFJ kinematics had similar patterns for both automatic and manual pipelines, apart from tibial internal/external rotations (Appendix B). Notably, tibial internal/external rotation had large variation for both automatic and manual pipelines (Fig. 3), due in part to presence of two distinct kinematics patterns: tibial internal or external rotation during TFJ flexion. Two distinct profiles of tibial internal or external rotation were found between pipelines in the deep TFJ flexion range for participant 2 and 7 (Appendix B: Fig. B2, B7) and for participant 4 (Appendix B: Fig. B4). Previous experiments have observed both tibial internal rotation [40] and external rotation [1,35] across passive TFJ flexion assessed *ex vivo*, suggesting both patterns were physiological. Indeed, in some cases, two patterns of tibial internal/external rotation were present in the Pareto solutions optimized from the same set of initial geometric parameters. Further constraints placed on predicted kinematics and/or ligament length variations might be required to regularize the tibial internal/external rotations. Despite the discrepancy of tibial internal/external rotations in deep TFJ flexion for some study subjects, physiological motion with reversal of the screw home motion (i.e., tibial internal rotation during initial TFJ flexion) was observed, except for participant 4, within the manual pipeline. Participants with larger TFJ kinematics errors (Appendix B: Figs. B2, B3, B7, and B8) did not have correspondingly higher geometric errors (e.g., ligament attachments and articular surfaces). As PFJ kinematics were driven by TFJ motions (due to constant length constraint for patellar tendon), large errors in TFJ kinematics likely contributed to PFJ kinematic errors (Appendix B: Figs. B2, B3, B7, and B8). Overall, the discrepancy between automatic and manual pipelines was most pronounced in deep TFJ flexion (>30° TFJ flexion). This was particularly evident for tibial internal/external rotations and, to some extent, for other DOF as well (Appendix B: Figs. B2, B3, B4, B7, and B8). It is worth noting the kinematic models in the current study (manual pipeline) were validated against *in vivo* measured kinematics through the initial TFJ flexion (approximately 0–25°) [3] (Appendix B). Thus, it cannot be concluded which pipeline was valid where there was a discrepancy between automatic and manual pipelines in the deep TFJ flexion of some DOF. Further *in vivo* experimental measurements made with the knee in deep TFJ flexion are needed to validate a larger range of predicted passive knee kinematics. The better agreement between manual and automatic pipelines across the shallow range of TFJ flexion provides more confidence in using the kinematic model for tasks such as walking stance, where deep knee flexion is uncommon.

The automatic pipeline presented in the current study to determine personalised TFJ and PFJ kinematics from joint geometry has several limitations. First, data were collected from typically developed healthy children and the modelling pipeline in pathological cases has not been assessed. This limits the use of our models to other populations such as those with bone deformities or conditions of the cartilages (e.g., defects) and ligaments (e.g., ACL deficiency). Second, TFJ and PFJ kinematic models were tuned (i.e., during geometric optimization) using previously reported measurements from adult cadaveric specimens (i.e., bone and ligaments kinematics) due to the lack of paediatric data, which may not represent the pattern of paediatric knee kinematics accurately. Third, due to the sensitivity of TFJ model to geometric parameters, geometric optimization was required to ensure physiological solutions. This optimization was informed by kinematics measured from cadaveric specimens [3,40] and acts to regularize the solutions, but limits personalisation as an individual's joint and ligament kinematics may not follow patterns reported in literature. Last, MOSPO implementation was slow and may not converge to a consistent set of Pareto solutions within a practical number of iterations. This suggests that running the algorithm multiple times could generate varying kinematics results, thereby

limiting reliability of the kinematics prediction. Future research may strive to reconsider core assumptions regarding rigidity of articular surfaces within TFJ and PFJ models as well as revisit MOPSO implementation to extract efficiencies or more robust behaviour. For instance, the geometric optimization could investigate including femoral spheres in addition to the current implementation of optimizing the tibial spheres, and/or to further regularize the TFJ internal/external rotation. In addition, future research may further extend the current automatic method by combining with technology that automatically segments joint geometry from medical imaging [20,37] or reconstructs joint geometry from anthropometric measurement via statistical shape modeling [41].

In conclusion, we presented a method to automatically determine passive TFJ and PFJ kinematics using 3D joint geometry. When compared to manual counterparts, the automatic pipeline determined geometric parameters with accuracy levels similar to human inter-operator reliability and predicted comparable TFJ and PFJ kinematics with no statistically significant difference (in 10 out of the 11 predicted DOF). This study demonstrated the feasibility of automatically personalising joint kinematics for musculoskeletal modelling, removed tedious manual processing, and reduced variability inherent to manual methods.

Conflict of interest statement

The authors whose names are listed immediately below certify that they have no affiliations with or involvement in any organization or

entity with any financial interest or non-financial interest in the subject matter or materials discussed in this manuscript.

CRediT authorship contribution statement

Beichen Shi: Writing – review & editing, Writing – original draft, Visualization, Software, Methodology, Investigation, Formal analysis. **Martina Barzan:** Writing – review & editing, Supervision, Software, Methodology, Investigation, Data curation, Conceptualization. **Azadeh Nasser:** Writing – review & editing, Supervision, Methodology, Conceptualization. **Jayishni N. Maharaj:** Writing – review & editing, Supervision, Methodology, Conceptualization. **Laura E. Diamond:** Writing – review & editing, Supervision, Methodology, Conceptualization. **David J. Saxby:** Writing – review & editing, Supervision, Methodology, Conceptualization.

Declaration of competing interest

The authors declare that they have no affiliations with or involvement in any organization or entity with any financial interest or non-financial interest in the subject matter or materials discussed in this manuscript.

Acknowledgements

This study was supported in part by a Griffith University Post-graduate Research Scholarship.

Appendix A

Tables A1, A2, A3

Table A1
Anatomical landmarks automatic determination error (mm).

	Median (ICQ)	Range [lower, upper]
Lateral femoral epicondyles	3.3 (1.0)	[1.5, 5.0]
Medial femoral epicondyles	4.9 (6.8)	[1.0, 12.7]
Femoral notch	5.4 (16.7)	[0.1, 30.4]
Lateral malleoli	1.8 (1.6)	[1.0, 5.0]
Medial malleoli	1.1 (0.2)	[0.8, 2.3]
Tibial joint centre	4.5 (0.4)	[2.4, 6.1]
Patella base	4.0 (2.0)	[1.5, 6.8]
Patellar apex	2.5 (1.4)	[1.2, 3.6]
Patellar lateral point	1.9 (2.1)	[0.8, 6.4]
Patellar medial point	4.2 (2.8)	[0.6, 5.2]
Patellar mid-ridge	4.0 (3.5)	[1.4, 7.2]
Hip joint centre	0.3 (0.2)	[0.1, 0.6]
All landmarks	2.8 (3.3)	[0.1, 30.4]

IQR: Interquartile range.

Table A2
Ligament automatic determination error (mm).

	Median (ICQ)	Range [lower, upper]
Ligament attachment sites distance error	1.9 (1.8)	[0.5, 5.9]
ACL L0 error	1.3 (1.7)	[0.2, 7.1]
PCL L0 error	1.2 (2.1)	[0.7, 4.0]
MCL L0 error	2.0 (2.5)	[0.2, 7.5]
LCL L0 error	1.3 (1.0)	[0.0, 3.7]
All L0 error	1.5 (1.8)	[0.0, 7.5]

IQR: Interquartile range.

Table A3

Joint articular surface determination root mean square error (mm).

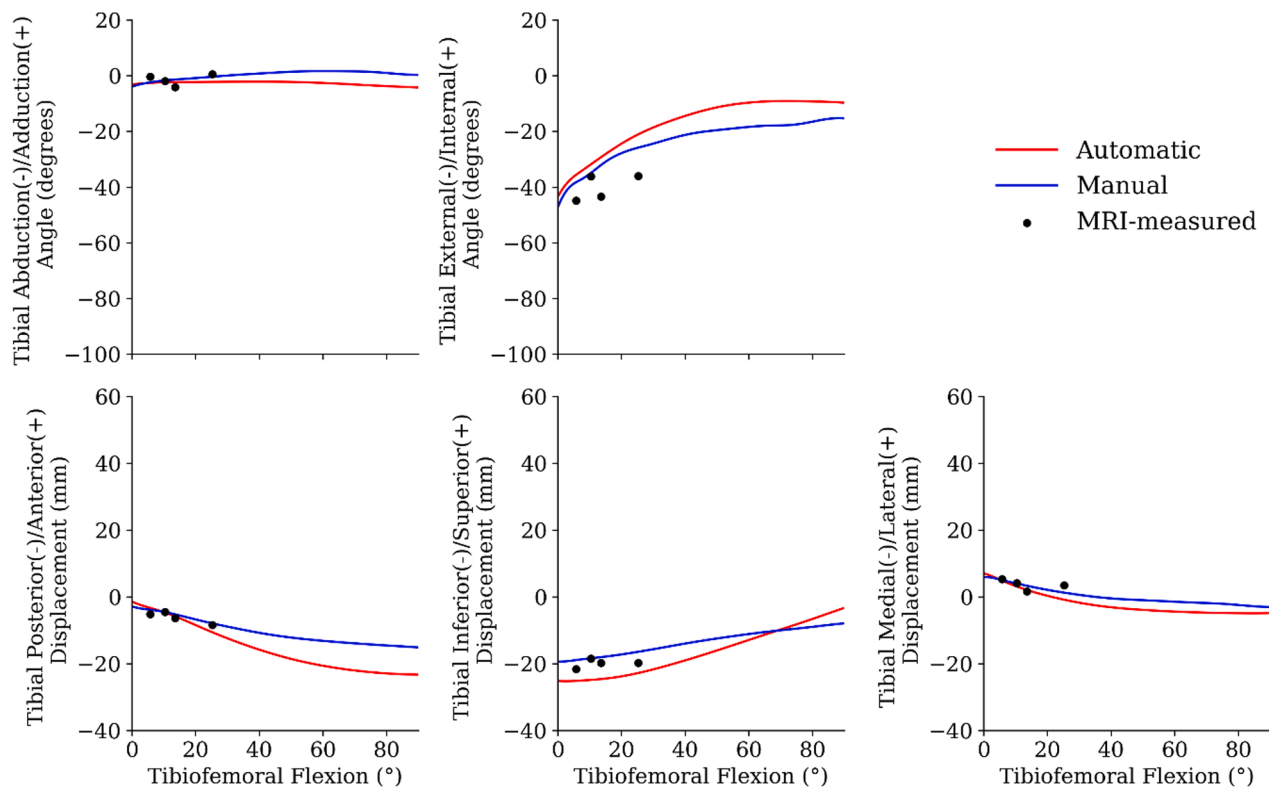
	Median (ICQ)	Range [lower, upper]
PFJ femoral articular surfaces	5.3 (3.3)	[1.5, 9.5]
TFJ femoral articular surface	0.8 (0.6)	[0.5, 4.5]
TFJ tibial articular surface	1.7 (1.0)	[0.8, 4.3]
All articular surfaces	1.7 (3.3)	[0.5, 4.5]

PFJ – patellofemoral joint; TFJ – tibiofemoral joint.

Appendix B. Predicted tibiofemoral and patellofemoral joint kinematics for each participant

The predicted tibiofemoral and patellofemoral joint kinematics from automatic and manual pipeline for each participant were plotted with the MRI-measured kinematics. In addition to the MRI-measured kinematics at neutral position, three additional MRI measures used for validation purposes in the previous study [3] were plotted. The readers are referred to the previous study for the details of the additional MRI scans [3]. It is worth noting that the MRI-measured kinematics were expressed using the same segment coordinate system as the manual pipeline (from manually determined anatomical landmarks). [Figs. B1, B2, B3, B4, B5, B6, B7, B8](#)

Tibiofemoral kinematics for participant 1



Patellofemoral kinematics for participant 1

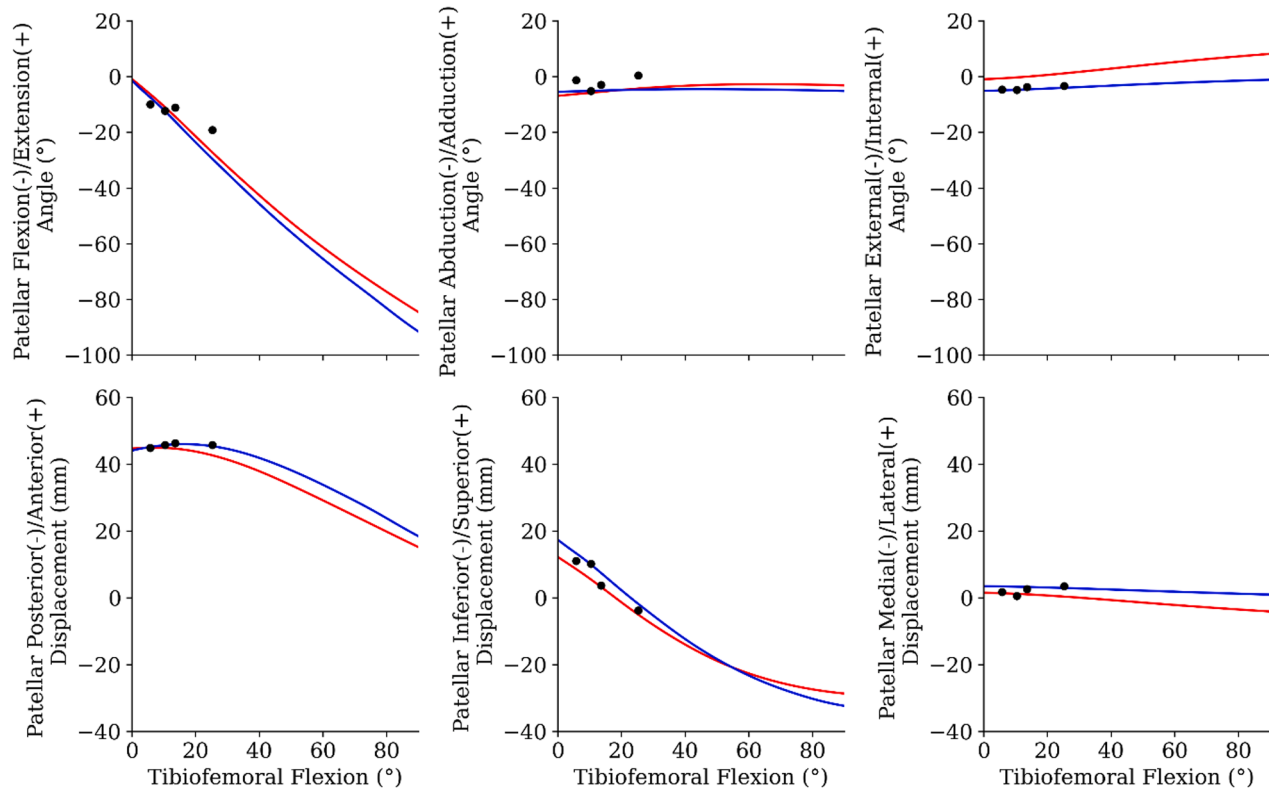
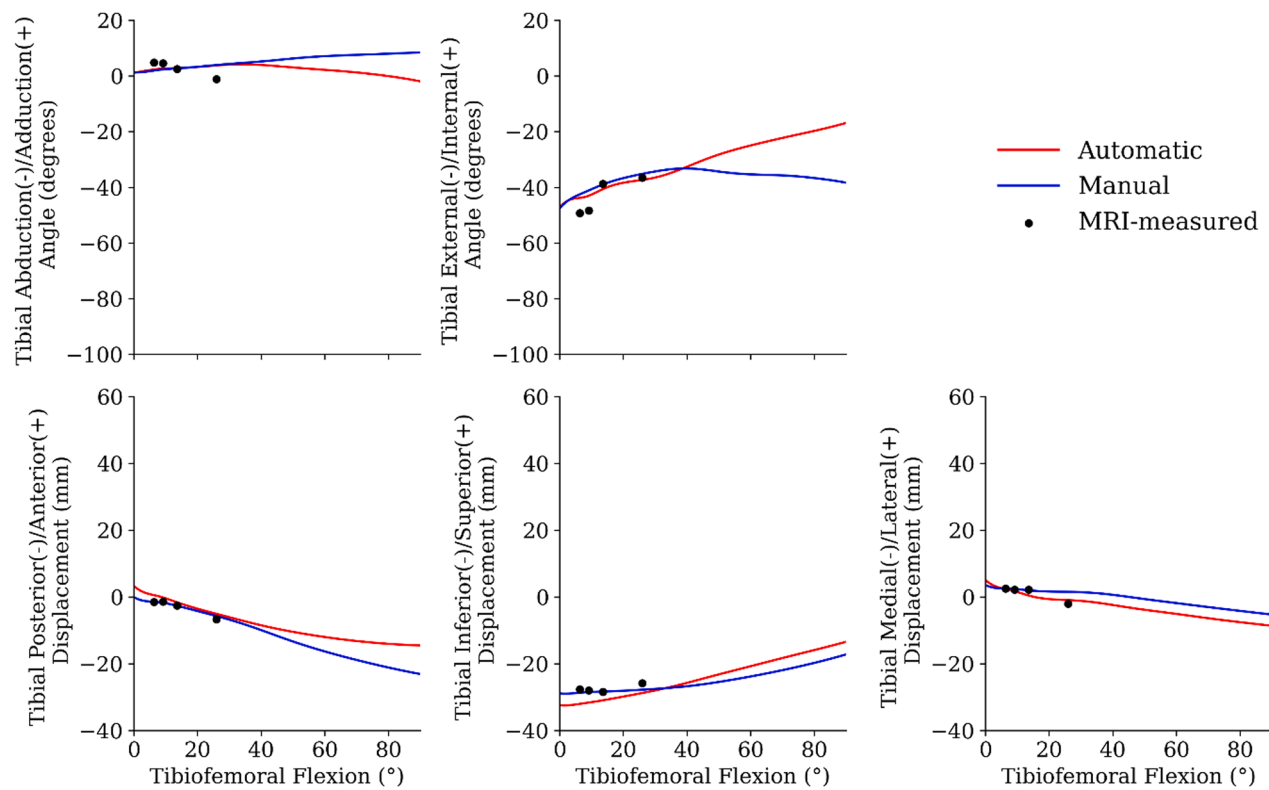


Fig. B1. Predicted tibiofemoral and patellofemoral joint kinematics from the automatic and manual pipeline of participant 1.

Tibiofemoral kinematics for participant 2



Patellofemoral kinematics for participant 2

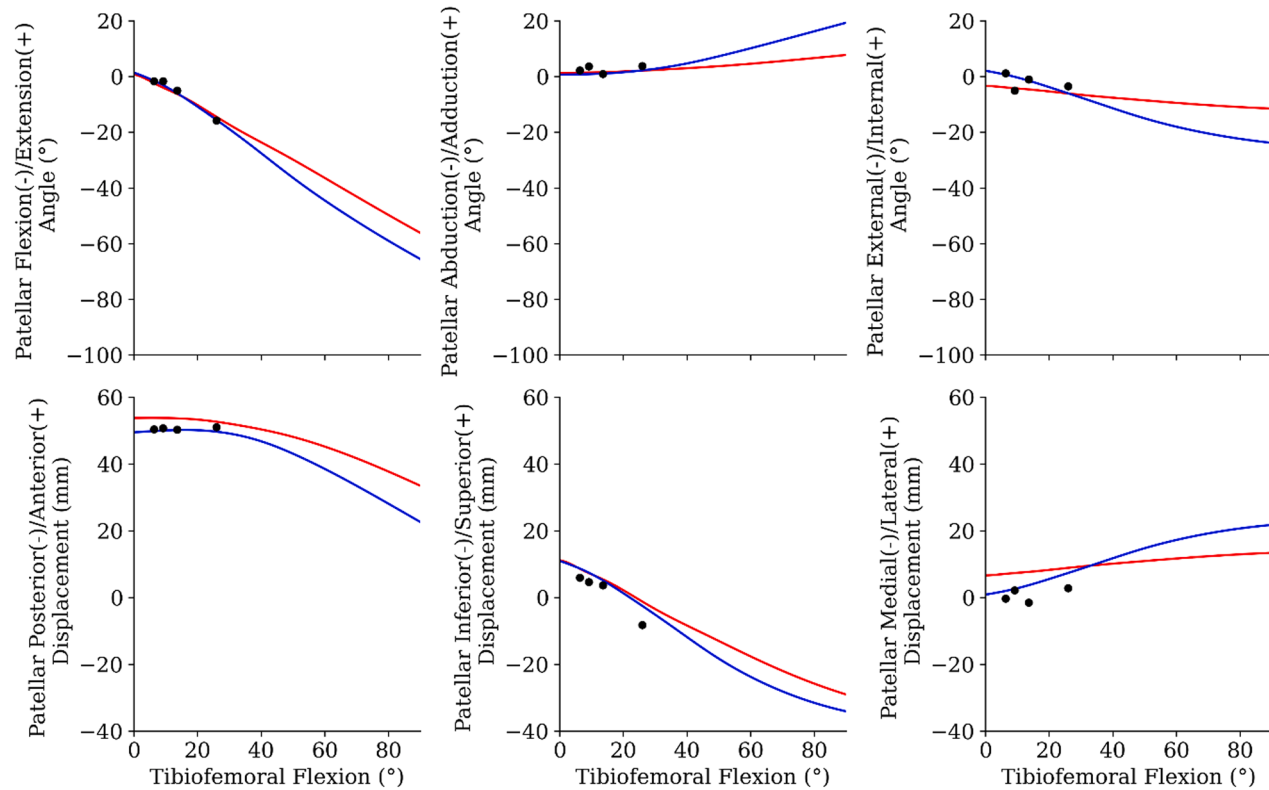
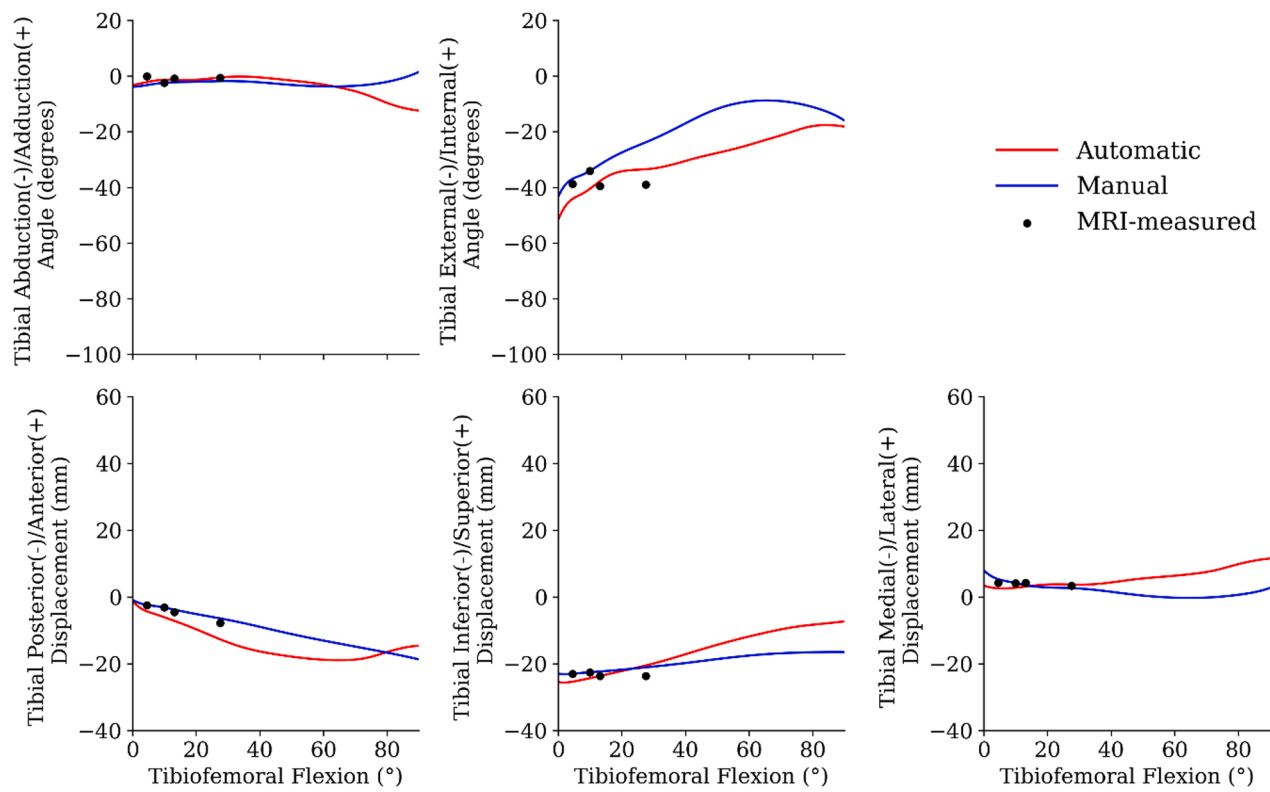


Fig. B2. Predicted tibiofemoral and patellofemoral joint kinematics from the automatic and manual pipeline of participant 2.

Tibiofemoral kinematics for participant 3



Patellofemoral kinematics for participant 3

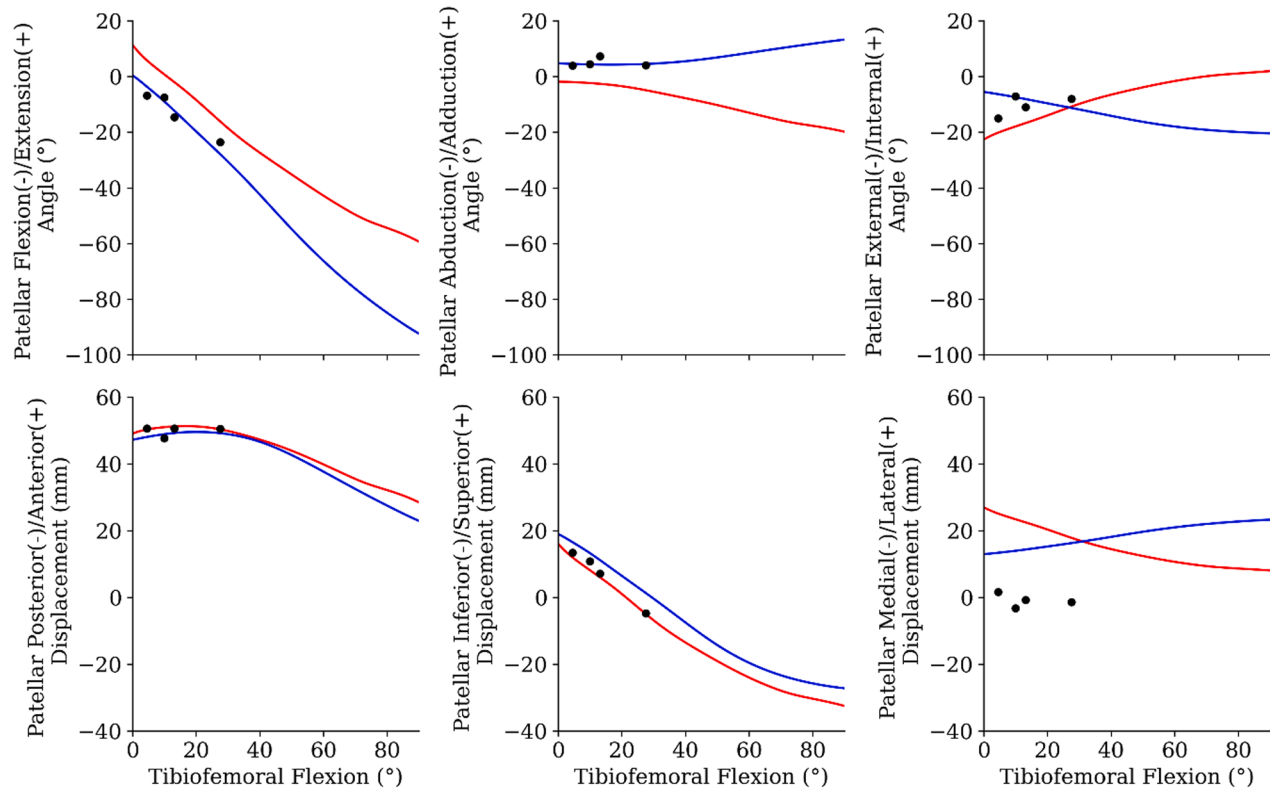
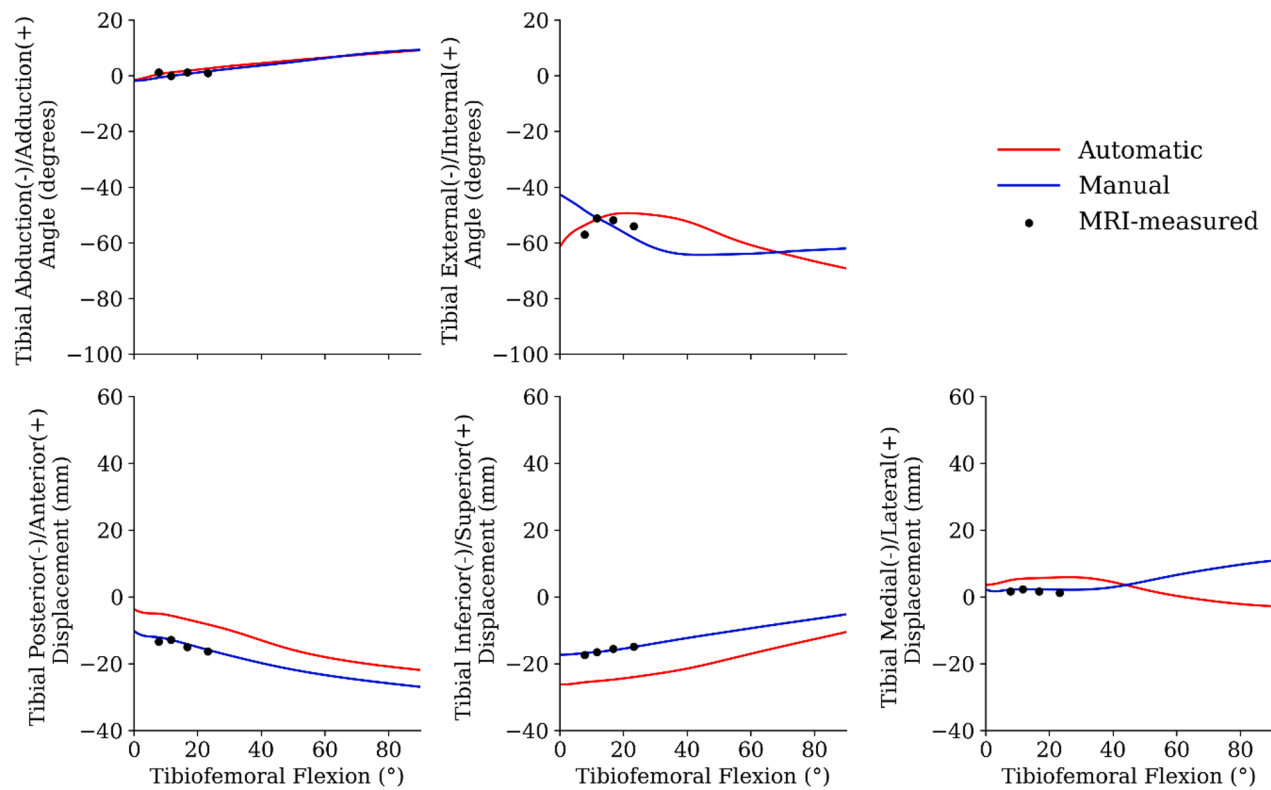


Fig. B3. Predicted tibiofemoral and patellofemoral joint kinematics from the automatic and manual pipeline of participant 3.

Tibiofemoral kinematics for participant 4



Patellofemoral kinematics for participant 4

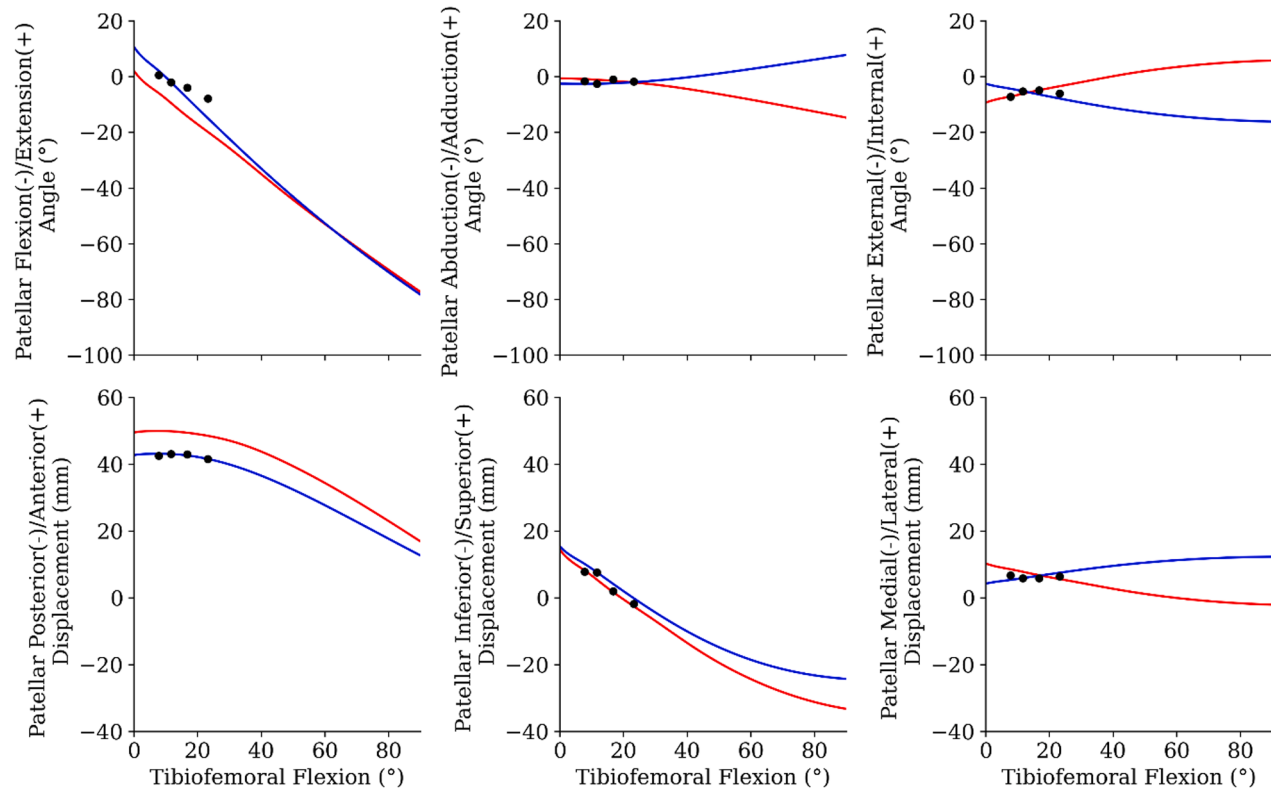
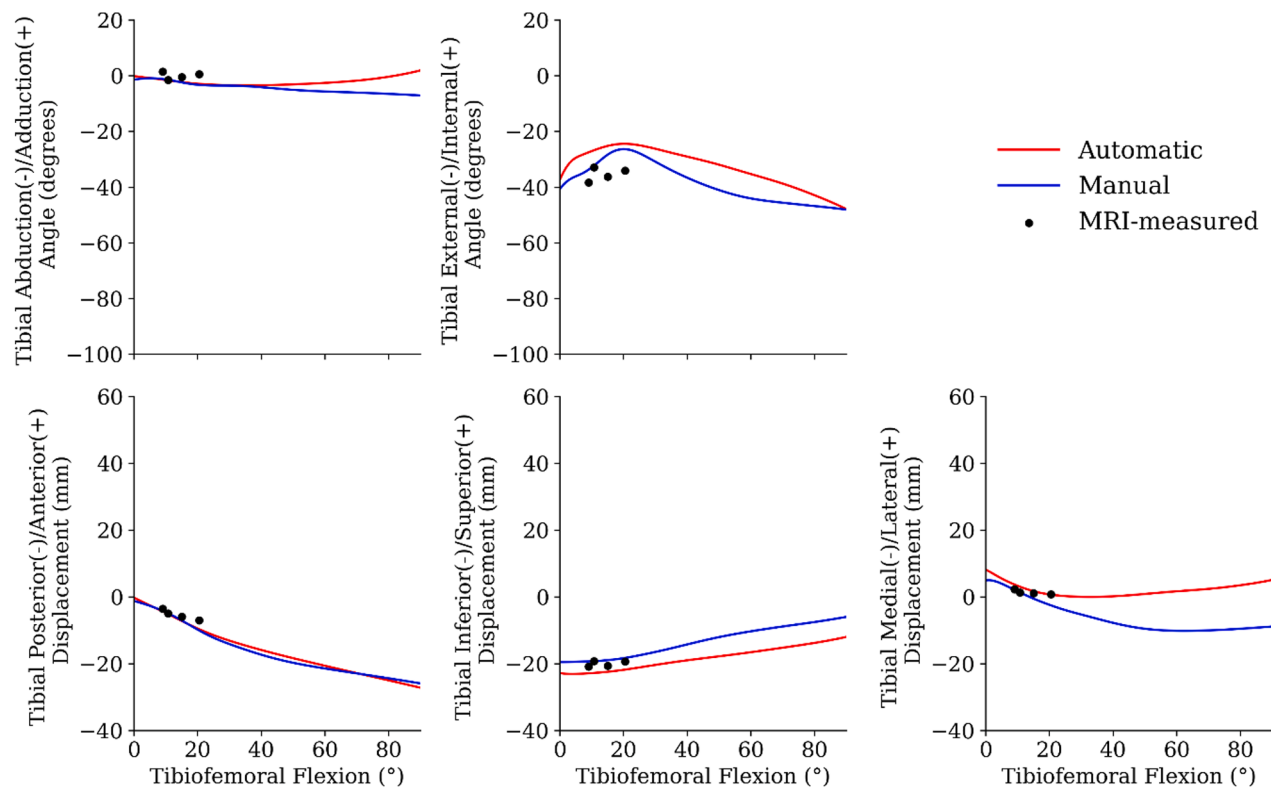


Fig. B4. Predicted tibiofemoral and patellofemoral joint kinematics from the automatic and manual pipeline of participant 4.

Tibiofemoral kinematics for participant 5



Patellofemoral kinematics for participant 5

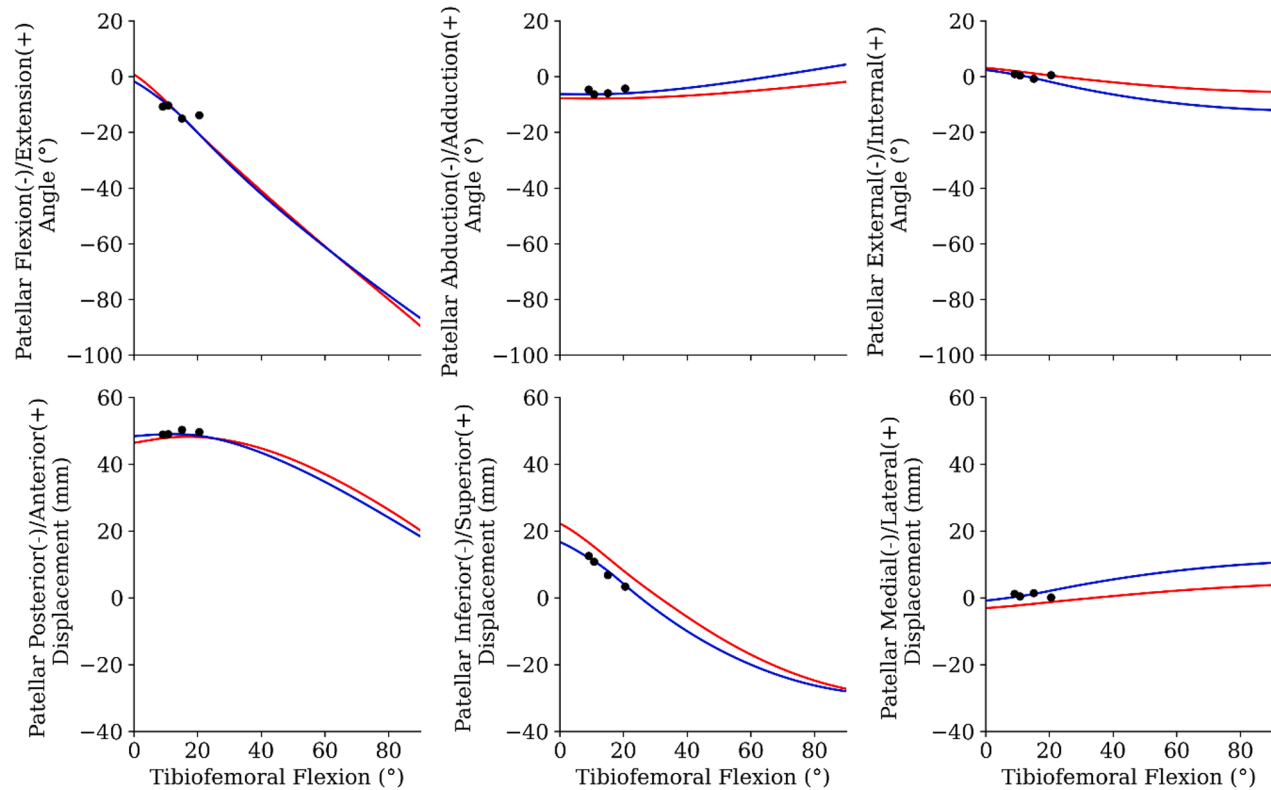
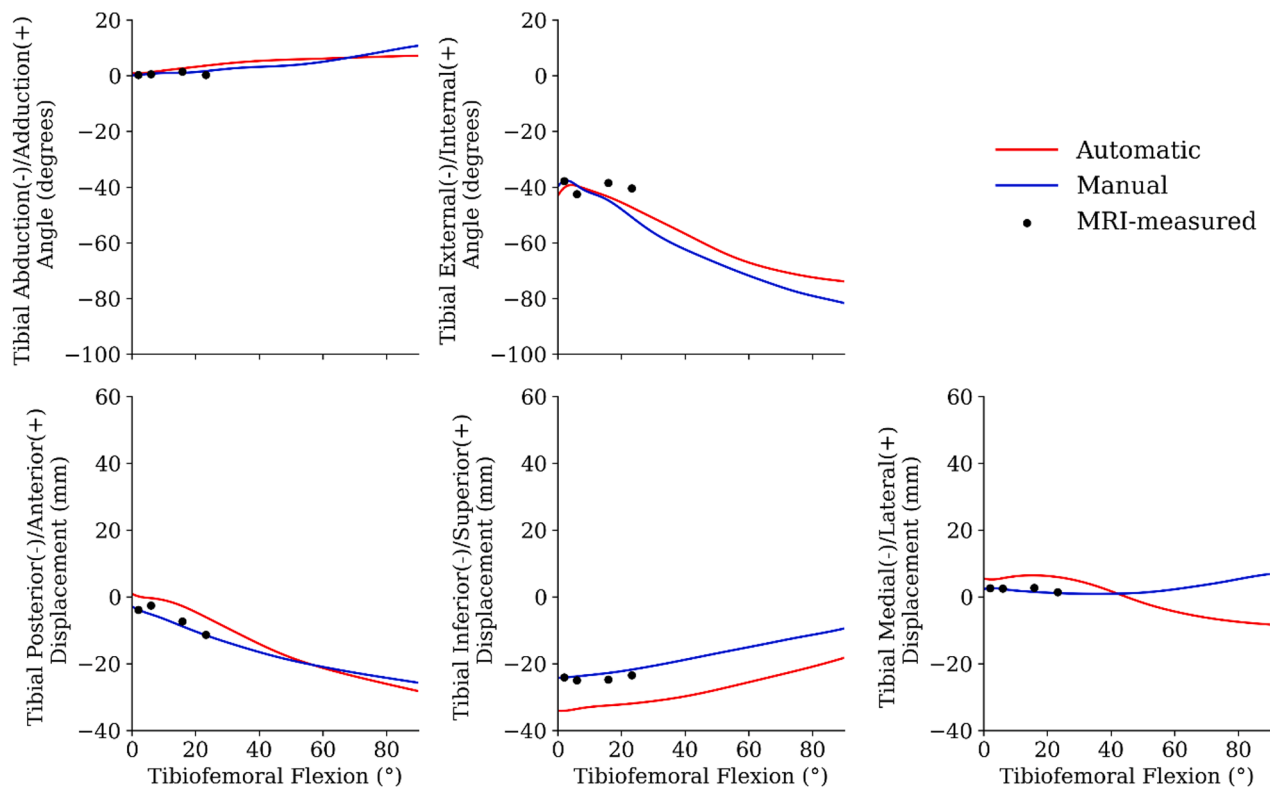


Fig. B5. Predicted tibiofemoral and patellofemoral joint kinematics from the automatic and manual pipeline of participant 5.

Tibiofemoral kinematics for participant 6



Patellofemoral kinematics for participant 6

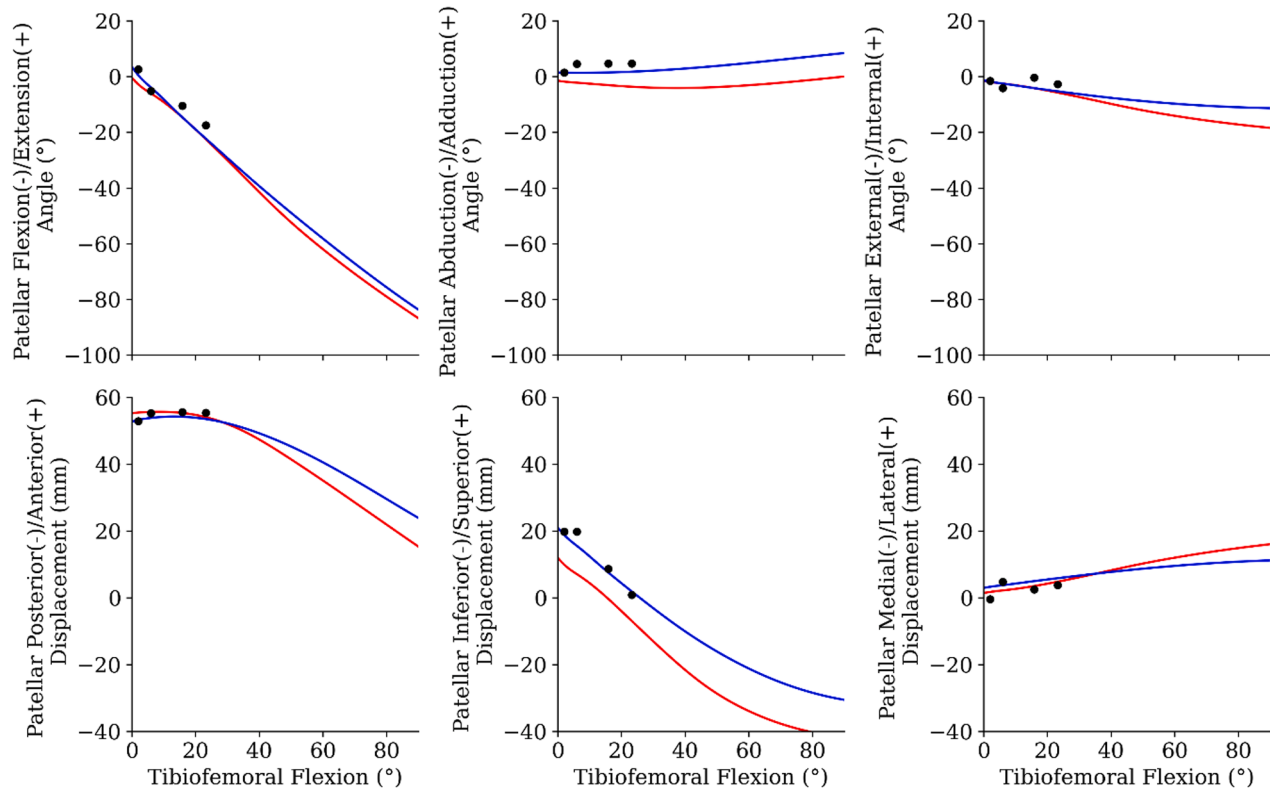
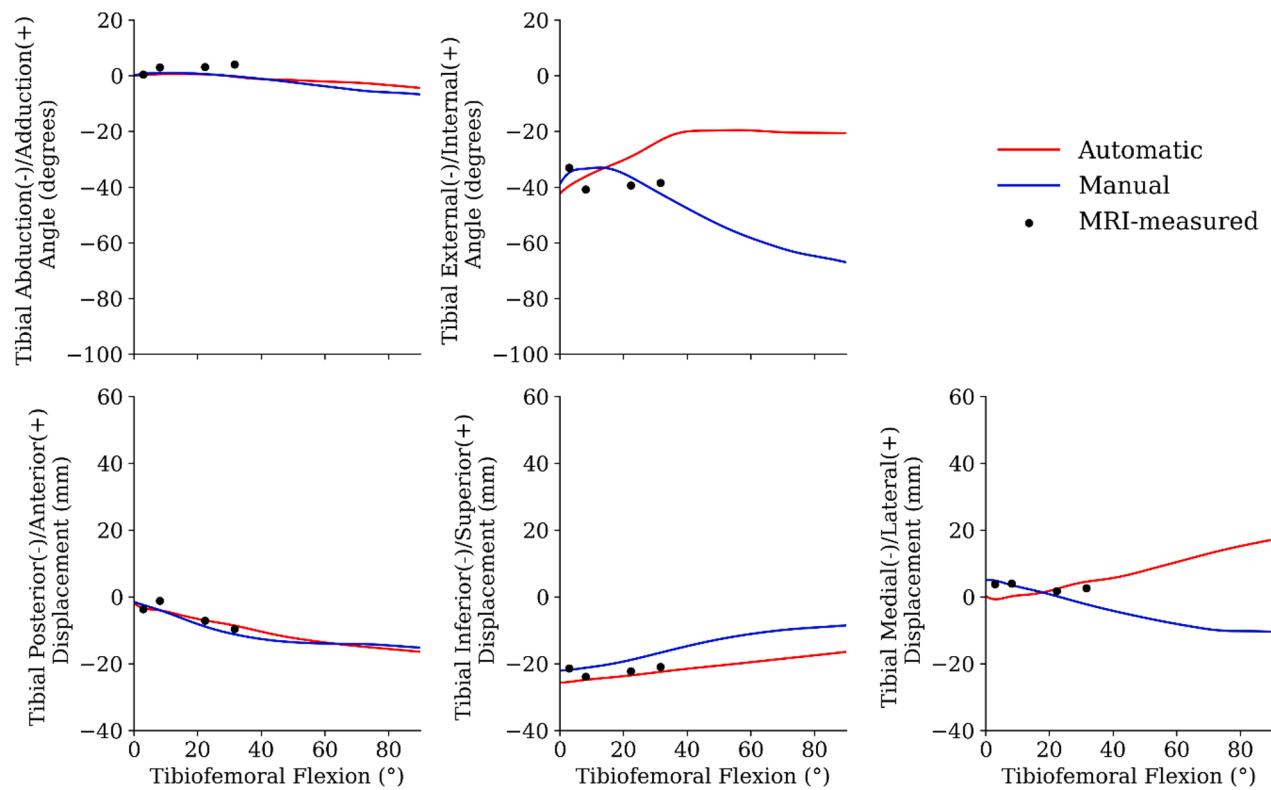


Fig. B6. Predicted tibiofemoral and patellofemoral joint kinematics from the automatic and manual pipeline of participant 6.

Tibiofemoral kinematics for participant 7



Patellofemoral kinematics for participant 7

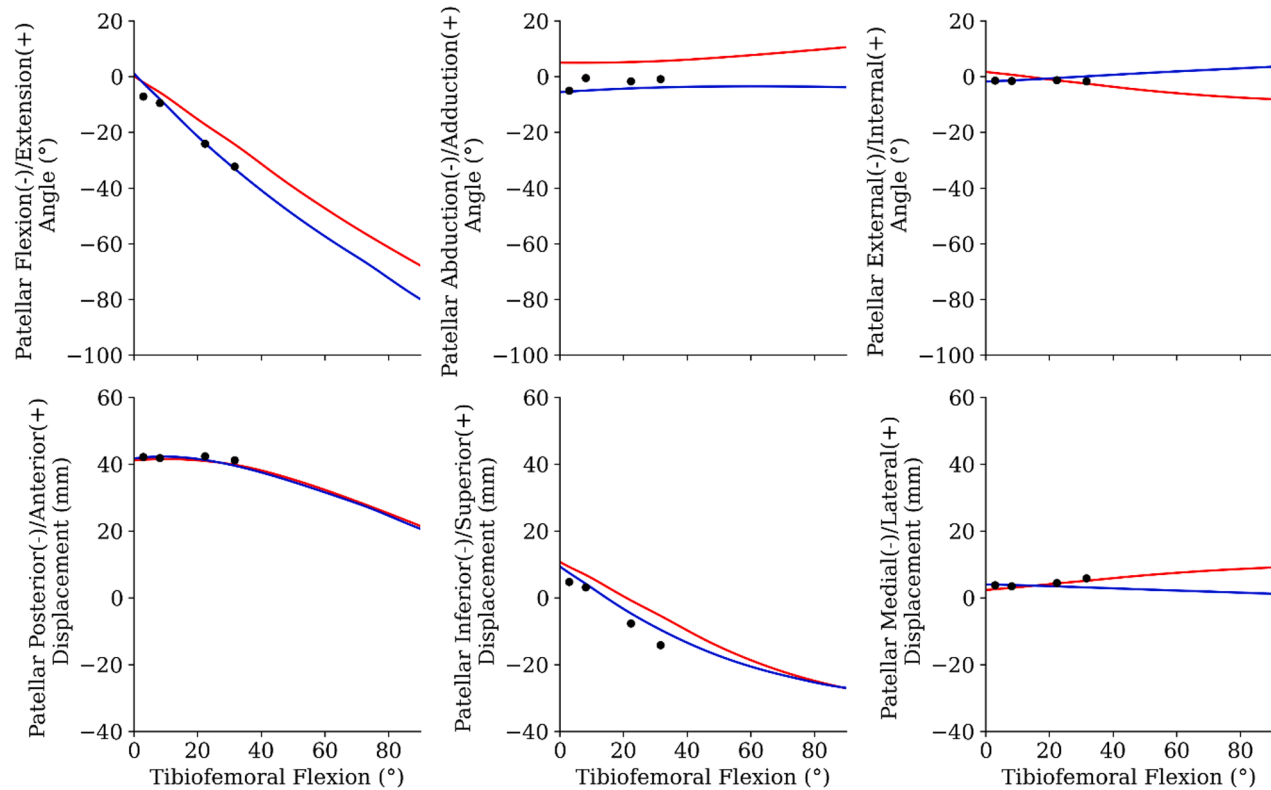
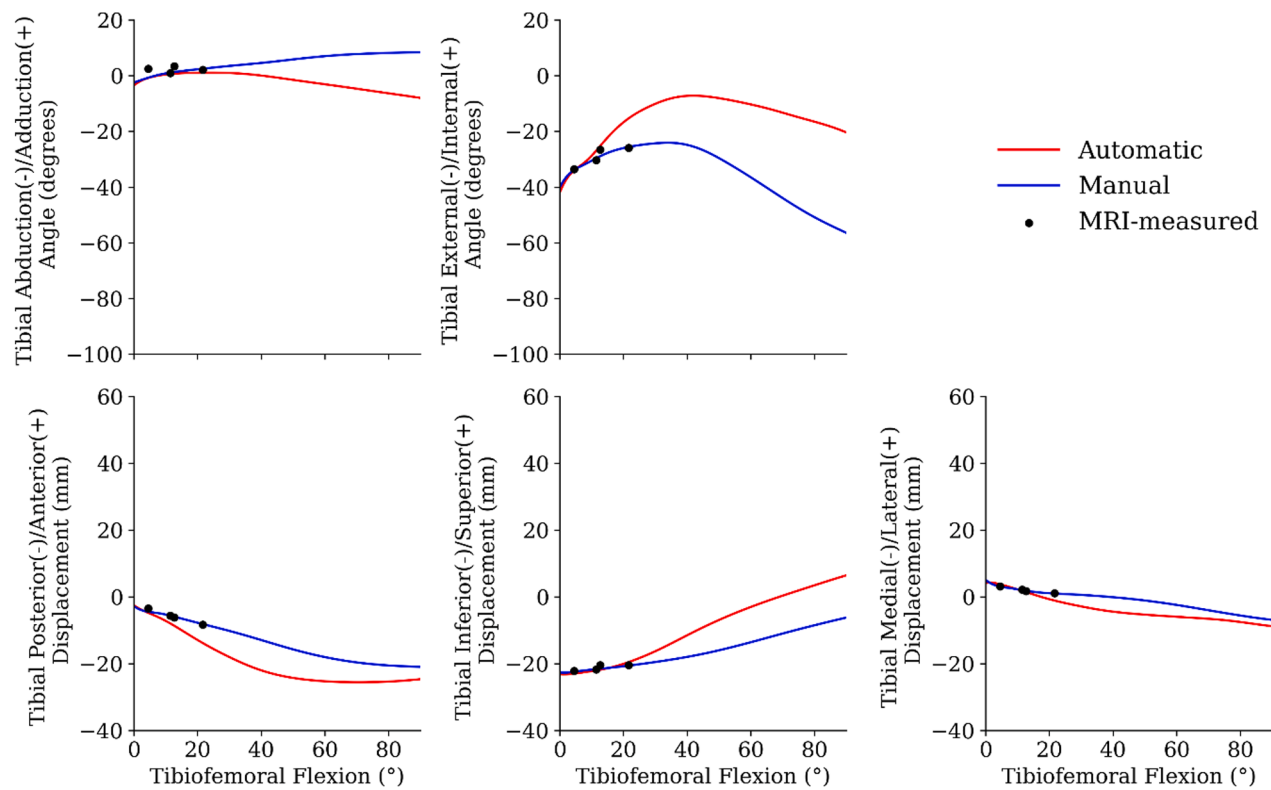


Fig. B7. Predicted tibiofemoral and patellofemoral joint kinematics from the automatic and manual pipeline of participant 7.

Tibiofemoral kinematics for participant 8



Patellofemoral kinematics for participant 8

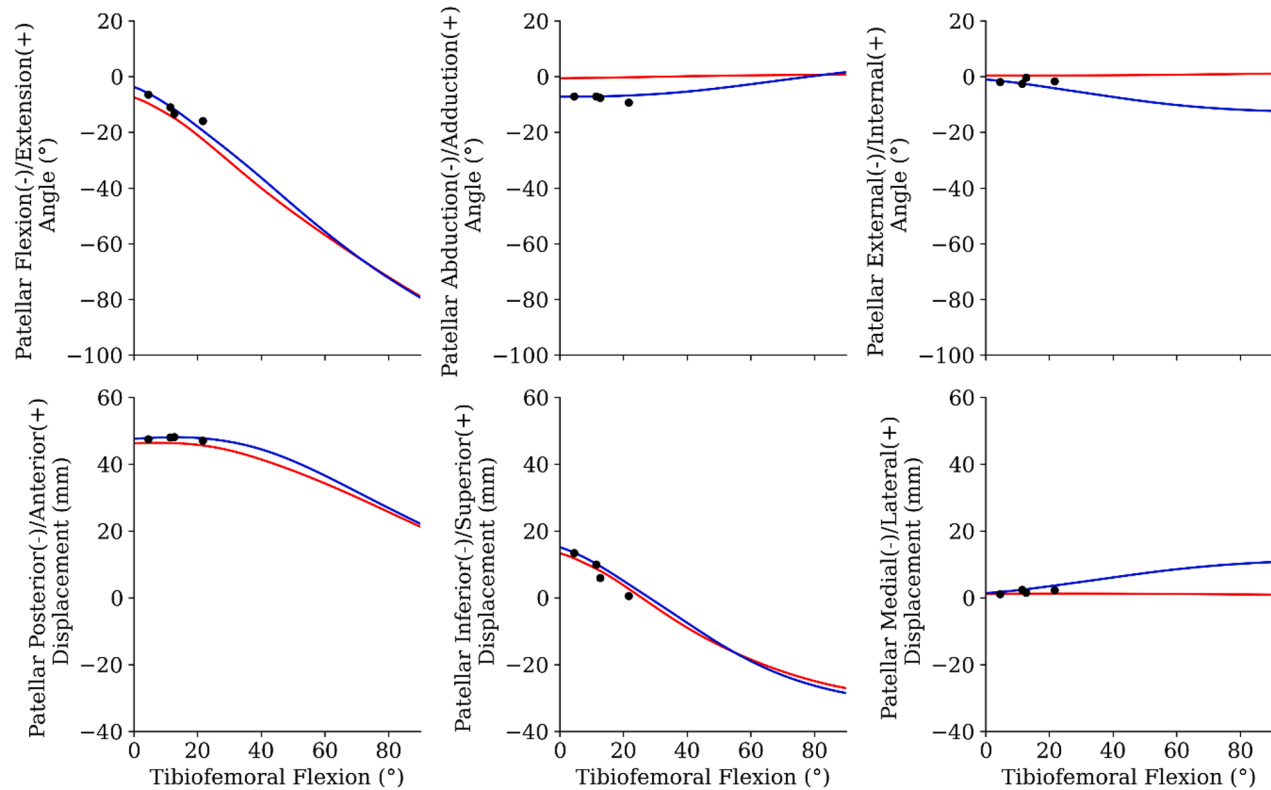


Fig. B8. Predicted tibiofemoral and patellofemoral joint kinematics from the automatic and manual pipeline of participant 8.

References

- [1] T.E. Andreassen, P.J. Laz, A. Erdemir, T.F. Besier, J.P. Halloran, C.W. Imhauser, S. Chokhandre, A. Schwartz, N.A. Nohouji, N.B. Rooks, M.T.Y. Schneider, S. Elmasry, W. Taylor, D.R. Hume, K.B. Shelburne, Deciphering the "Art" in Modeling and Simulation of the Knee Joint: assessing Model Calibration Workflows and Outcomes, *J. Biomech. Eng.* 145 (12) (2023), <https://doi.org/10.1115/1.4063627>.
- [2] C. Anglin, K.C. Ho, J.L. Briard, C. de Lambilly, C. Plaskos, E. Nodwell, E. Stindel, In vivo patellar kinematics during total knee arthroplasty, *Computer Aided Surgery* 13 (6) (2008) 377–391, <https://doi.org/10.3109/10929080802594563>.
- [3] M. Barzan, L. Modenese, C.P. Carty, S. Maine, C.A. Stockton, N. Sancisi, A. Lewis, J. Grant, D.G. Lloyd, S. Brito da Luz, Development and validation of subject-specific pediatric multibody knee kinematic models with ligamentous constraints, *J. Biomech.* 93 (2019) 194–203, <https://doi.org/10.1016/j.jbiomech.2019.07.001>.
- [4] C. Belvedere, F. Catani, A. Ensini, J.L. Moctezuma De La Barrera, A. Leardini, Patellar tracking during total knee arthroplasty: an in vitro feasibility study, *Knee Surgery, Sports Traumatology, Arthroscopy* 15 (8) (2007) 985–993, <https://doi.org/10.1007/s00167-007-0320-1>.
- [5] C. Belvedere, A. Ensini, A. Feliciangeli, F. Cenni, V. D'Angeli, S. Giannini, A. Leardini, Geometrical changes of knee ligaments and patellar tendon during passive flexion, *J. Biomech.* 45 (11) (2012) 1886–1892, <https://doi.org/10.1016/j.jbiomech.2012.05.029>.
- [6] E. Bergamini, H. Pillet, J. Hausselle, P. Thoreux, S. Guerard, V. Camomilla, A. Cappozzo, W. Skalli, Tibio-femoral joint constraints for bone pose estimation during movement using multi-body optimization, *Gait, Posture* 33 (4) (2011) 706–711, <https://doi.org/10.1016/j.gaitpost.2011.03.006>.
- [7] L. Blankevoort, R. Huiskes, A. De Lange, Recruitment of Knee Joint Ligaments, *J. Biomech.* 113 (1) (1991) 94–103, <https://doi.org/10.1115/1.2894090>.
- [8] M. Brehler, G. Thawait, J. Kaplan, J. Ramsay, M.J. Tanaka, S. Demehri, J. H. Siewersdén, W. Bzibjewski, Atlas-based algorithm for automatic anatomical measurements in the knee, *J. Med. Imaging* 6 (02) (2019) 1, <https://doi.org/10.1117/1.jmi.6.2.026002>.
- [9] S. Brito Da Luz, L. Modenese, N. Sancisi, P.M. Mills, B. Kennedy, B.R. Beck, D. G. Lloyd, Feasibility of using MRIs to create subject-specific parallel-mechanism joint models, *J. Biomech.* 53 (2017) 45–55, <https://doi.org/10.1016/j.jbiomech.2016.12.018>.
- [10] A. Cappozzo, F. Catani, A. Leardini, M.G. Benedetti, U.D. Croce, Position and orientation in space of bones during movement: experimental artefacts, *Clin. Biomech. (Bristol, Avon)* 11 (2) (1996) 90–100, [https://doi.org/10.1016/0268-0033\(95\)00046-1](https://doi.org/10.1016/0268-0033(95)00046-1).
- [11] R. Chen, Y. Ma, N. Chen, L. Liu, Z. Cui, Y. Lin, W. Wang, Structure-Aware Long Short-Term Memory Network for 3D Cephalometric Landmark Detection, *IEEE Trans. Med. ImAGING* 41 (7) (2022) 1791–1801, <https://doi.org/10.1109/tmi.2022.3149281>.
- [12] J. Clément, R. Dumas, N. Hagemeister, J.A. De Guise, Soft tissue artifact compensation in knee kinematics by multi-body optimization: performance of subject-specific knee joint models, *J. Biomech.* 48 (14) (2015) 3796–3802, <https://doi.org/10.1016/j.jbiomech.2015.09.040>.
- [13] C.A.C. Coello, G.T. Pulido, M.S. Lechuga, Handling multiple objectives with particle swarm optimization, *IEEE Trans. Evolutionary Computation* 8 (3) (2004) 256–279, <https://doi.org/10.1109/TEVC.2004.826067>.
- [14] M. Conconi, N. Sancisi, V. Parenti-Castelli, Prediction of Individual Knee Kinematics From an MRI Representation of the Articular Surfaces, *IEEE Trans. Biomedical Engineering* 68 (3) (2021) 1084–1092, <https://doi.org/10.1109/tbme.2020.3018113>.
- [15] M. Conconi, N. Sancisi, V. Parenti-Castelli, Exploiting Reciprocity Between Constraints and Instantaneous Motion to Reconstruct Individual Knee Kinematics, *Adv. Robot Kinematics* (2022). Cham.
- [16] A.K. Dastgerdi, A. Esrafilian, C.P. Carty, A. Nasseri, M. Barzan, R.K. Korhonen, I. Astori, W. Hall, D.J. Saxby, Sensitivity analysis of paediatric knee kinematics to the graft surgical parameters during anterior cruciate ligament reconstruction: a sequentially linked neuromusculoskeletal-finite element analysis, *Comput. Methods Programs Biomed.* 248 (2024) 108132, <https://doi.org/10.1016/j.cmpb.2024.108132>.
- [17] R. Di Gregorio, V. Parenti-Castelli, A spatial mechanism with higher pairs for modelling the human knee joint, *J. Biomech. Eng.* 125 (2) (2003) 232–237, <https://doi.org/10.1115/1.1559895>.
- [18] M.C.M. Fischer, S.A.G.A. Grothues, J. Habor, M. De La Fuente, K. Radermacher, A robust method for automatic identification of femoral landmarks, axes, planes and bone coordinate systems using surface models, *Sci. Rep.* 10 (1) (2020), <https://doi.org/10.1038/s41598-020-77479-z>.
- [19] M.C.M. Fischer, F. Kroob, J. Habor, K. Radermacher, A robust method for automatic identification of landmarks on surface models of the pelvis, *Sci. Rep.* 9 (1) (2019), <https://doi.org/10.1038/s41598-019-49573-4>.
- [20] S.W. Flannery, A.M. Kiapour, D.J. Edgar, M.M. Murray, B.C. Fleming, Automated magnetic resonance image segmentation of the anterior cruciate ligament, *J. Orthopaedic Research* 39 (4) (2021) 831–840, <https://doi.org/10.1002/j.or.24926>.
- [21] X. Gasparutto, N. Sancisi, E. Jacquelin, V. Parenti-Castelli, R. Dumas, Validation of a multi-body optimization with knee kinematic models including ligament constraints, *J. Biomech.* 48 (6) (2015) 1141–1146, <https://doi.org/10.1016/j.jbiomech.2015.01.010>.
- [22] E.S. Grood, W.J. Suntay, A joint coordinate system for the clinical description of three-dimensional motions: application to the knee, *J. Biomech. Eng.* 105 (2) (1983) 136–144, <https://doi.org/10.1115/1.3138397>.
- [23] H. Jacinto, S. Valette, R. Prost, Multi-atlas automatic positioning of anatomical landmarks, *J. Vis. Commun. Image Represent.* 50 (2018) 167–177.
- [24] S. Kai, T. Sato, Y. Koga, G. Omori, K. Kobayashi, M. Sakamoto, Y. Tanabe, Automatic construction of an anatomical coordinate system for three-dimensional bone models of the lower extremities – Pelvis, femur, and tibia, *J. Biomech.* 47 (5) (2014) 1229–1233, <https://doi.org/10.1016/j.biomech.2013.12.013>.
- [25] H.Y. Kim, K.J. Kim, D.S. Yang, S.W. Jeung, H.G. Choi, W.S. Choy, Screw-Home Movement of the Tibiofemoral Joint during Normal Gait: three-Dimensional Analysis, *Clin. Orthop. Surg.* 7 (3) (2015) 303, <https://doi.org/10.4055/cios.2015.7.3.303>.
- [26] C.P.S. Kulseng, V. Nainamalai, E. Grøvik, J.-T. Geitung, A. Årøen, K.-I. Gjesdal, Automatic segmentation of human knee anatomy by a convolutional neural network applying a 3D MRI protocol, *BMC. Musculoskelet. Disord.* 24 (1) (2023), <https://doi.org/10.1186/s12891-023-06153-y>.
- [27] A. Leardini, C. Belvedere, F. Nardini, N. Sancisi, M. Conconi, V. Parenti-Castelli, Kinematic models of lower limb joints for musculo-skeletal modelling and optimization in gait analysis, *J. Biomech.* 62 (2017) 77–86, <https://doi.org/10.1016/j.jbiomech.2017.04.029>.
- [28] A. Leardini, Z. Sawacha, G. Paolini, S. Ingrosso, R. Nativo, M.G. Benedetti, A new anatomically based protocol for gait analysis in children, *Gait, Posture* 26 (4) (2007) 560–571, <https://doi.org/10.1016/j.gaitpost.2006.12.018>.
- [29] Z. Li, J. Yang, X. Li, K. Wang, J. Han, P. Yang, Comparing two different automatic methods to measure femoral neck-shaft angle based on PointNet++ network, *Sci. Rep.* 12 (1) (2022), <https://doi.org/10.1038/s41598-022-16695-1>.
- [30] Z. Liu, A. Zhou, V. Fauveau, J. Lee, P. Marcadis, Z.A. Fayad, J.J. Chan, J. Gladstone, X. Mei, M. Huang, Deep Learning for Automated Measurement of Patellofemoral Anatomic Landmarks, *Bioengineering* 10 (7) (2023) 815, <https://doi.org/10.3390/bioengineering10070815>.
- [31] L. Modenese, J.-B. Renault, Automatic Generation of Personalised Skeletal Models of the Lower Limb from Three-Dimensional Bone Geometries, *J. Biomech.* (2020) 110186, <https://doi.org/10.1016/j.jbiomech.2020.110186>.
- [32] F. Moissenet, L. Chèze, R. Dumas, A 3D lower limb musculoskeletal model for simultaneous estimation of musculo-tendon, joint contact, ligament and bone forces during gait, *J. Biomech.* 47 (1) (2014) 50–58, <https://doi.org/10.1016/j.jbiomech.2013.10.015>.
- [33] Y. Morishige, K. Harato, S. Oki, K. Kaneda, Y. Niki, M. Nakamura, T. Nagura, Four-dimensional computed tomographic analysis of screw home movement in patients with anterior cruciate ligament deficient knee — A 3D-3D registration technique, *Skeletal Radiol.* 51 (8) (2022) 1679–1685, <https://doi.org/10.1007/s00256-021-03986-3>.
- [34] F. Nardini, C. Belvedere, N. Sancisi, M. Conconi, A. Leardini, S. Durante, V. Parenti-Castelli, An Anatomical-Based Subject-Specific Model of In-Vivo Knee Joint 3D Kinematics From Medical Imaging, *Applied Sciences* 10 (6) (2020) 2100, <https://doi.org/10.3390/app10062100>.
- [35] A. Ottoboni, V. Parenti-Castelli, N. Sancisi, C. Belvedere, A. Leardini, Articular surface approximation in equivalent spatial parallel mechanism models of the human knee joint: an experiment-based assessment, *Proceedings of the Institution of Mechanical Engineers, Part H: Journal of Engineering in Medicine* 224 (9) (2010) 1121–1132, <https://doi.org/10.1243/09544119jeim684>.
- [36] V. Parenti-Castelli, R. Di Gregorio, Parallel Mechanisms Applied to the Human Knee Passive Motion Simulation, in: J. Lenarčić, M.M. Stanisic (Eds.), *Advances in Robot Kinematics*, Springer, Netherlands, 2000, pp. 333–344, https://doi.org/10.1007/978-94-011-4120-8_35.
- [37] Y. Peng, H. Zheng, P. Liang, L. Zhang, F. Zaman, X. Wu, M. Sonka, D.Z. Chen, KCB-Net: a 3D knee cartilage and bone segmentation network via sparse annotation, *Med. Image Anal.* 82 (2022) 102574, <https://doi.org/10.1016/j.media.2022.102574>.
- [38] J.-B. Renault, G. Aüllö-Rasser, M. Donnez, S. Parratte, P. Chabrand, Articular-surface-based automatic anatomical coordinate systems for the knee bones, *J. Biomech.* 80 (2018) 171–178, <https://doi.org/10.1016/j.jbiomech.2018.08.028>.
- [39] N. Sancisi, V. Parenti-Castelli, A New Kinematic Model of the Passive Motion of the Knee Inclusive of the Patella, *J. Mech. Robot.* 3 (4) (2011), <https://doi.org/10.1115/1.4004890>.
- [40] N. Sancisi, V. Parenti-Castelli, A novel 3D parallel mechanism for the passive motion simulation of the patella-femur-tibia complex, *Meccanica* 46 (1) (2011) 207–220, <https://doi.org/10.1007/s11012-010-9405-x>.
- [41] B. Shi, M. Barzan, A. Nasseri, C.P. Carty, D.G. Lloyd, G. Davico, J.N. Maharaj, L. E. Diamond, D.J. Saxby, Development of predictive statistical shape models for paediatric lower limb bones, *Comput. Methods Programs Biomed.* 225 (2022) 107002, <https://doi.org/10.1016/j.cmpb.2022.107002>.
- [42] I. Sintini, N. Sancisi, V. Parenti-Castelli, Comparison between anatomical and approximate surfaces in a 3D kinetostatic model of the knee for the study of the unloaded and loaded joint motion, *Meccanica* 53 (1–2) (2018) 7–20, <https://doi.org/10.1007/s11012-017-0696-z>.
- [43] K. Subburaj, B. Ravi, M. Agarwal, Automated identification of anatomical landmarks on 3D bone models reconstructed from CT scan images, *Comput. Med. Imaging Graphics* 33 (5) (2009) 359–368, <https://doi.org/10.1016/j.compmedimag.2009.03.001>.
- [44] E. Theilen, A. Rörich, T. Lange, S. Bendak, C. Huber, H. Schmal, K. Izadpanah, J. Georgii, Validation of a Finite Element Simulation for Predicting Individual Knee

- Joint Kinematics, IEEE Open. J. Eng. Med. Biol. 5 (2024) 125–132, <https://doi.org/10.1109/OJEMB.2023.3258362>.
- [45] G.T. Yamaguchi, F.E. Zajac, A planar model of the knee joint to characterize the knee extensor mechanism, *J. Biomech.* 22 (1) (1989) 1–10, [https://doi.org/10.1016/0021-9290\(89\)90179-6](https://doi.org/10.1016/0021-9290(89)90179-6).
- [46] J. Zhang, D. Ackland, J. Fernandez, Point-cloud registration using adaptive radial basis functions, *Comput. Methods Biomed. Engin.* 21 (7) (2018) 498–502, <https://doi.org/10.1080/10255842.2018.1484914>.